

4-2018

Experimental and modeling of CO₂ removal from gas mixtures using membrane contractors packed with glass beads.

Farah O.S. Abuhatab

Follow this and additional works at: https://scholarworks.uaeu.ac.ae/chem_petro_theses



Part of the [Chemical Engineering Commons](#)

Recommended Citation

Abuhatab, Farah O.S., "Experimental and modeling of CO₂ removal from gas mixtures using membrane contractors packed with glass beads." (2018). *Chemical and Petroleum Engineering Theses*. 5.
https://scholarworks.uaeu.ac.ae/chem_petro_theses/5

This Thesis is brought to you for free and open access by the Chemical and Petroleum Engineering at Scholarworks@UAEU. It has been accepted for inclusion in Chemical and Petroleum Engineering Theses by an authorized administrator of Scholarworks@UAEU. For more information, please contact fadl.musa@uaeu.ac.ae.



جامعة الإمارات العربية المتحدة
United Arab Emirates University

United Arab Emirates University

College of Engineering

Department of Chemical and Petroleum Engineering

EXPERIMENTAL AND MODELING OF CO₂ REMOVAL FROM
GAS MIXTURES USING MEMBRANE CONTACTORS PACKED
WITH GLASS BEADS

Farah O. S. Abuhatab

This thesis is submitted in partial fulfillment of the requirements for the degree of
Master of Science in Chemical Engineering

Under the Supervision of Professor Mohamed H. Al-Marzouqi

April 2018

Approval of the Master Thesis

This Master Thesis is approved by the following Examining Committee Members:

- 1) Advisor (Committee Chair): Mohamed H. Al-Marzouqi

Title: Professor

Department of Chemical and Petroleum Engineering

College of Engineering

Signature  _____

Date 07/05/2018

- 2) Member: Mohammed H. Al-Saleh

Title: Associate Professor

Department of Chemical and Petroleum Engineering

College of Engineering

Signature  _____

Date 7/5/2018

- 3) Member (External Examiner): Hyungwoong Ahn

Title: Senior Lecturer

Department of Chemical Engineering

Institution: The University of Edinburgh, UK

Signature  _____

Date 8/5/2018

Prof. Basim Abu-Jdayil

Abstract

Natural gas is one of the major natural resources in UAE which carries significant amounts of acid gases. For the purpose of utilizing or liquefying, the gas must be pre-treated by separating the major non-hydrocarbon gases, namely CO₂. Typical CO₂ separation processes involve separation using sorbents or solvent, cryogenic or membrane. Among these processes, the chemical absorption considered to be the most effective process to remove CO₂. However, this process carries several drawbacks such as flooding, foaming, entraining, channeling, and most importantly high capital and operating costs.

An integrated unit called gas absorption membrane (GAM) consists of combining chemical absorption process with membrane contactors has also been investigated. The heat exchanger concept is being applied by membrane gas absorptions it allows the indirect contact between the two fluids; the gas mixture flows in the inner side of hydrophobic microporous membrane fibers while the liquid absorbent flows in the outer side of the microporous membrane. At the pores opening of the membrane, a gas-liquid interface is formed where the gas is being absorbed and reacted.

The aim of this study is to investigate the performance of gas absorption membrane (GAM) in capturing carbon dioxide at elevated pressure (up to 25 bars) in which the shell compartment is packed with glass beads. The purpose of packing is to enhance fluid mixing and reduce resistance in the liquid phase. A commercial microporous hollow fiber membranes (PFA) was used in this investigation. Different parameters were studied and compared with modules without beads; these parameters include the effect of gas and liquid flow rates, solvent type (NaOH,

MEA, EDA, DEA, and DETA), inlet solvent concentration and beads size. All these parameters were studied as a function of pressure. Additionally, the overall mass transfer coefficients obtained from the experimental data were compared with those of the modeling.

The results indicated up to % 20 improvements in % CO₂ removal in packed modules as compared with the modules without beads. As expected, increasing the gas flow rate had a negative effect on % CO₂ removal while increasing solvent inlet concentration enhanced % CO₂ removal. Increasing the inlet liquid flow rate and the type of solvents had almost no effect on % CO₂ removal. Decreasing the beads size increases the solvent velocity in the module and thus increases the % CO₂ removal. The experimental overall mass transfer coefficient agreed well with those calculated from the theory which proves the reliability of experimental data.

Keywords: Natural gas, Carbon dioxide, hollow fiber membrane contactors, Absorption, microporous hollow fiber membranes, gas-liquid interface.

Copyright © 2018 Farah O.S. Abuhatab
All Rights Reserved

Advisory Committee

1) Advisor: Mohamed H. Al-Marzouqi

Title: Professor, Vice Dean

Department of Chemical and Petroleum Engineering

College of Engineering

2) Co-advisor: Sayed A. Marzouk

Title: Professor

Department of Chemistry

College of Science

3) Member: Mohammed H. Al-Saleh

Title: Associate Professor

Department of Chemical and Petroleum Engineering

College of Engineering

Abstract

Natural gas is one of the major natural resources in UAE which carries significant amounts of acid gases. For the purpose of utilizing or liquefying, the gas must be pre-treated by separating the major non-hydrocarbon gases, namely CO₂. Typical CO₂ separation processes involve separation using sorbents or solvent, cryogenic or membrane. Among these processes, the chemical absorption considered to be the most effective process to remove CO₂. However, this process carries several drawbacks such as flooding, foaming, entraining, channeling, and most importantly high capital and operating costs.

An integrated unit called gas absorption membrane (GAM) consists of combining chemical absorption process with membrane contactors has also been investigated. The heat exchanger concept is being applied by membrane gas absorptions it allows the indirect contact between the two fluids; the gas mixture flows in the inner side of hydrophobic microporous membrane fibers while the liquid absorbent flows in the outer side of the microporous membrane. At the pores opening of the membrane, a gas-liquid interface is formed where the gas is being absorbed and reacted.

The aim of this study is to investigate the performance of gas absorption membrane (GAM) in capturing carbon dioxide at elevated pressure (up to 25 bars) in which the shell compartment is packed with glass beads. The purpose of packing is to enhance fluid mixing and reduce resistance in the liquid phase. A commercial microporous hollow fiber membranes (PFA) was used in this investigation. Different parameters were studied and compared with modules without beads; these parameters include the effect of gas and liquid flow rates, solvent type (NaOH,

MEA, EDA, DEA, and DETA), inlet solvent concentration and beads size. All these parameters were studied as a function of pressure. Additionally, the overall mass transfer coefficients obtained from the experimental data were compared with those of the modeling.

The results indicated up to % 20 improvements in % CO₂ removal in packed modules as compared with the modules without beads. As expected, increasing the gas flow rate had a negative effect on % CO₂ removal while increasing solvent inlet concentration enhanced % CO₂ removal. Increasing the inlet liquid flow rate and the type of solvents had almost no effect on % CO₂ removal. Decreasing the beads size increases the solvent velocity in the module and thus increases the % CO₂ removal. The experimental overall mass transfer coefficient agreed well with those calculated from the theory which proves the reliability of experimental data.

Keywords: Natural gas, Carbon dioxide, hollow fiber membrane contactors, Absorption, microporous hollow fiber membranes, gas-liquid interface.

Title and Abstract (in Arabic)

دراسة معملية لعمليات امتصاص غاز ثاني أكسيد الكربون من خلال المقاطع العشائية المعبأة بالكريات الزجاجية

الملخص

يعتبر الغاز الطبيعي أحد أهم الموارد الطبيعية في دولة الإمارات العربية المتحدة. يحتوي الغاز الطبيعي على بعض الغازات الحمضية، تحديداً غاز ثاني أكسيد الكربون الذي بدوره يحمل تأثير سلبي على عمليات تنقية الغاز الطبيعي. لهذا السبب وجب تنقية الغاز الطبيعي قبل تسويله أو استخدامه. تنوعت تقنيات فصل غاز ثاني أكسيد الكربون عن الغاز الطبيعي مثل عمليات الفصل باستخدام المواد الماصة أو المذيبات، المواد المبردة أو الأغشية. ومن بين هذه العمليات تعتبر عملية الامتصاص الكيميائي الأكثر فعالية في امتصاص وفصل غاز ثاني أكسيد الكربون. ولكن ذلك لا يمنع من وجود بعض العيوب عند استخدامها كالمشاكل التشغيلية وارتفاع رأس المال وتكاليف التشغيل.

تم استحداث تقنية جديدة تمزج ما بين الامتصاص الكيميائي والأغشية أطلق عليها اسم وحدة أغشية امتصاص الغاز. في هذه الوحدة يطبق مفهوم وحدة المبادل الحراري الذي يسمح بالاتصال الغير المباشر بين الغاز والمذيب. بالإضافة إلى ذلك وجود الغشاء ذو المسامية الصغيرة والذي يعمل كوسيط بين الغاز والمذيب بحيث يسمح بالتقاء الموائع عند المسامات وتفاعلاها.

الهدف من الأطروحة هو التحقيق في أداء وحدة أغشية امتصاص الغاز المعبأة بالكريات الزجاجية في امتصاص غاز ثاني أكسيد الكربون تحت تأثير الضغط العالي (يصل إلى 25). تكمن الغاية من تعبئة الوحدة بالكريات الزجاجية في تحسين المزج وتقليل المقاومة في السائل المستخدم. تم استخدام نوع معين من الأغشية المستوردة (PFA) ونوع واحد من المذيبات

(NaOH). شملت الأطروحة دراسة بعض العوامل المختلفة بدلالة الضغط، كتأثير الغاز ومعدلات تدفق السائل المدخل، نوع المذيبات (NaOH, MEA, EDA, DEA and DETA)، تركيز المذيب وحجم الكريات الزجاجية. بالإضافة إلى ذلك، تمت مقارنة معاملات نقل الكتلة الكلية التي تم الحصول عليها من البيانات التجريبية مع المعاملات النظرية.

أظهرت النتائج تحسن في إزالة غاز ثاني أكسيد الكربون إلى ما يصل إلى 20 % في الوحدات المعبأة بالكريات مقارنة مع الوحدات الخالية من الكريات. وكما كان متوقعا، فإن زيادة معدل تدفق الغاز كان له تأثير سلبي على نسبة إزالة غاز ثاني أكسيد الكربون في كلا الودعتين (المعبأة بالكريات الزجاجية والخالية منها). كذلك أدى زيادة تركيز المذيبات إلى ارتفاع نسبة إزالة غاز ثاني أكسيد الكربون كما هو متوقع. إن ارتفاع معدل تدفق السائل المدخل واختلاف نوع المذيبات لم يحمل أي تأثير على نسبة إزالة غاز ثاني أكسيد الكربون. في المقابل، فإن تقليل حجم الكريات الزجاجية زاد من سرعة المذيبات في الوحدة، وبالتالي أدى إلى زيادة نسبة إزالة غاز ثاني أكسيد الكربون. علاوة على ذلك، فإن الأطروحة قدمت توافق بين معاملات نقل الكتلة الكلية التي أوجدت من النظريات مع المحسوبة من البيانات التجريبية.

مفاهيم البحث الرئيسية: الغاز الطبيعي، وحدة أغشية امتصاص الغاز، المذيب، الموائع، معاملات نقل الكتلة الكلية، غاز ثاني أكسيد الكربون، الكريات الزجاجية

Acknowledgements

I would like to express my special thanks of gratitude to my supervisor Prof. Mohammed Al Marzooqi. His door was always open whenever I ran into a trouble spot or had a question about my research or writing. I could not have imagined having a better advisor and mentor for my Master study. As well as my Co-advisor Prof. Sayed Marzouk who gave me the golden opportunity to do this wonderful project and also helped me in doing a lot of Research and I came to know about so many new things. Without their passionate participation and input, the project could not have been successfully conducted.

Secondly, special thanks goes to Dr. Nadia who supported my work and helped me get results of better quality. She definitely provided me with the tools that I needed to choose the right direction and successfully complete my thesis.

I am also grateful to the members of my committee (Dr. Mohammed Al Saleh and Dr. Basim Abu Jadayel) for their patience and support in overcoming numerous obstacles I have been facing through my research. In addition, I would like to thank my parents and friends who helped me a lot in finalizing this project within the limited time frame.

Finally, I must express my very profound gratitude to my Husband for providing me with unfailing support and continuous encouragement throughout my years of study. This accomplishment would not have been possible without him.

Dedication

To my beloved parents and husband

Table of Contents

Title	i
Declaration of Original Work	ii
Copyright	iii
Advisory Committee	iv
Approval of the Master Thesis	v
Abstract	vii
Title and Abstract (in Arabic)	ix
Acknowledgements	xi
Dedication	xii
Table of Contents	xiii
List of Tables.....	xv
List of Figures	xvi
List of Abbreviations.....	xviii
Chapter 1: Introduction	1
1.1 Overview	1
1.2 Statement of the problem	2
1.3 Research objectives	3
1.4 Limitations of the Study	3
1.5 Organization of the thesis.....	4
Chapter 2: Relevant Literature	5
2.1 Conventional gas separation techniques	5
2.2 Potential candidate for gas separation-Gas absorption membrane (GAM)	7
2.2.1 Membrane gas separation at high pressure.....	8
2.2.2 Packed membrane gas contactors.....	9
2.3 Membrane characteristics.....	10
2.4 Membrane absorbent compatibility.....	12
2.5 Membrane wetting	12
2.6 Membrane mass transfer coefficient	14
Chapter 3: Experimental Work	16
3.1 Construction and preparation of hollow fiber membrane contactors	16
3.1.1 The mechanical part	16
3.1.2 The chemical part	20
3.2 Experimental set-up	23

Chapter 4: Results and Discussion.....	25
4.1 Construction and fabrication of custom-made HFMCs	25
4.1.1 Selection of membrane	25
4.1.2 Selection of solvent/gas mixture	28
4.1.3 Selection of flow direction	29
4.2 Experimental investigation of CO ₂ removal using PFA fibers.....	31
4.2.1 Effect of packing HFMCs with beads	31
4.2.2 The effect of glass beads size	33
4.2.3 The effect of varying gas flow rate	35
4.2.4 The effect of varying liquid flow rate	37
4.2.5 Effect of amine type	40
4.2.6 Inlet solvent concentration	43
4.3 Evaluation of the overall mass transfer coefficients for chemical absorption	45
4.3.1 Theoretical mass transfer coefficient	45
4.3.2 Experimental mass transfer coefficient	49
4.3.3 Individual MTC for module A & B based on theory.	49
4.3.4 Overall MTC for module A & B theoretically and experimentally	51
Chapter 5: Conclusions	56
References	57
Appendices	64
Appendix A: Calculations of %CO ₂ Removal and CO ₂ Flux	64
Appendix B: Calculations of theoretical Mass Transfer Coefficient	66
B.1 The overall mass transfer coefficient.....	66
B.2 The individual mass transfer coefficient	68
Appendix C: Calculations of CO ₂ loading.	81

List of Tables

Table 1: Characteristics of selected hollow fiber membranes	11
Table 2: Membrane-absorbent compatibility	12
Table 3: The number of beads used for each size	21
Table 4: Membrane characteristics	27
Table 5: The calculated velocity for each module	34
Table 6: Chemical structure of the used amines solvent.....	41
Table 7: Physical properties used in the calculation	48
Table 8: Characteristics of PFA fiber	48
Table 9: Beads used in the module	49
Table 10: Parameters used in %CO ₂ removal and CO ₂ flux calculations.....	65
Table 11: Parameters used to calculate the theoretical overall MTC.....	67
Table 12: Parameters used to calculate Leveque's correlation	68
Table 13: Parameters used to calculate mass transfer in membrane side	71
Table 14: Parameters used to calculate hydraulic diameter	73
Table 15: Parameters used to calculate Hatta number and enhancement factor	75
Table 16: Parameters used to calculate velocity of shell	78
Table 17: Parameters used to calculate correlation (18)	79
Table 18: parameters to calculate CO ₂ loading.....	82

List of Figures

Figure 1: Schematic diagram of CO ₂ absorption plant.	6
Figure 2: Disk structure.....	18
Figure 3: Cover disk structure.....	19
Figure 4: Filter structure.....	20
Figure 5: Module structure drawing.....	22
Figure 6: Front side of the module.....	22
Figure 7: Experimental setup used for CO ₂ removal at elevated pressure.....	23
Figure 8: The outer surface of PFA fiber showing the pore diameter.	27
Figure 9: Custom-made HFMCs without glass beads.....	30
Figure 10: Custom-made HFMCs packed with glass beads.	30
Figure 11: Effect of packing the HFMC with beads (1 mm) on the chemical absorption of %CO ₂ using PFA-HFM at fixed gas flow rate (2000 mL/min) and aqueous sodium hydroxide flow rates (20 mL/min).	32
Figure 12: The effect of packing the HFMC with beads (1 mm) in terms of flux using PFA-HFM at fixed gas flow rate (2000 mL/min) and aqueous sodium hydroxide flow rates (20 mL/min).	33
Figure 13: The effect of varying beads size (0.25, 1 and 2 mm) on the chemical absorption of %CO ₂ using PFA-HFM at fixed gas flow rate (2000 mL/min) and aqueous sodium hydroxide flow rates (20 mL/min).	34
Figure 14: The effect of beads size in terms of velocity using PFA-HFM at fixed gas flow rate (2000 mL/min), aqueous sodium hydroxide flow rates (20 mL/min) and pressure of 15 bars.	35
Figure 15: The effect of varying gas flow rate (1000, 2000 and 3000 mL/min) on module (A).	36
Figure 16: The effect of varying gas flow rate (1000, 2000 and 3000 mL/min) on module (B).	37
Figure 17: The effect of varying liquid flow rate (10, 20 and 30 mL/min) on module (A) using PFA-HFM at a fixed gas flow rate (2000 mL/min).	38
Figure 18: The effect of varying liquid flow rate (10, 20 and 30 mL/min) on module (B) using PFA-HFM at a fixed gas flow rate (2000 mL/min).	39
Figure 19: The effect of liquid flow rate on modules (A) & (B) in terms of velocity using PFA-HFM at a fixed gas flow rate (2000 mL/min), aqueous sodium hydroxide flow rates (10, 20 & 30 mL/min) and pressure of 10 bars.	40

Figure 20: The effect of amine type on module (A) using PFA-HFM at fixed gas flow rate (2000 mL/min) and aqueous sodium hydroxide flow rates (20 mL/min).	42
Figure 21: The effect of amine type on module (B) using PFA-HFM at fixed gas flow rate (2000 mL/min) and aqueous sodium hydroxide flow rates (20 mL/min).	43
Figure 22: The effect of inlet solvent concentration on module (A) using PFA-HFM at fixed gas flow rate (2000 mL/min) and aqueous sodium hydroxide flow rates (20 mL/min).	44
Figure 23: The effect of inlet solvent concentration on module (B) using PFA-HFM at fixed gas flow rate (2000 mL/min) and aqueous sodium hydroxide flow rates (20 mL/min).	44
Figure 24: Individual MTC for module (A) & (B) for gas film and membrane using PFA-HFM at fixed gas flow rate (2000 mL/min) and aqueous sodium hydroxide flow rates (20 mL/min).	50
Figure 25: Individual MTC for module (A) & (B) for liquid film using PFA-HFM at fixed gas flow rate (2000 mL/min) and aqueous sodium hydroxide flow rates (20 mL/min).	50
Figure 26: Comparison between overall mass transfer coefficients based on theoretical and experimental correlations for module (A) using PFA-HFM at fixed gas flow rate (2000 mL/min) and aqueous sodium hydroxide flow rates (20 mL/min).	52
Figure 27: Comparison between overall mass transfer coefficients based on theoretical and experimental correlations for module (B) using PFA-HFM at fixed gas flow rate (2000 mL/min) and aqueous sodium hydroxide flow rates (20 mL/min).	52
Figure 28: Theoretical overall MTC using PFA-HFM at fixed gas flow rate (2000 mL/min) and aqueous sodium hydroxide flow rates (20 mL/min) for module (A) and (B).	53
Figure 29: Experimental overall MTC using PFA-HFM at fixed gas flow rate (2000 mL/min) and aqueous sodium hydroxide flow rates (20 mL/min) for module (A) and (B).	54
Figure 30: Overall MTC using correlation (7) & (8) using PFA-HFM at fixed gas flow rate (2000 mL/min) and aqueous sodium hydroxide flow rates (20 mL/min).	55

List of Abbreviations

Al_2O_3	Aluminium oxide
CCS	Carbon Capture and Storage
CH_4	Methane
CNT	Carbon nanotubes
CO_2	Carbon dioxide
DEA	Diethanolamine
DETA	Diethylenetriamine
di	Inside diameter of membrane
do	Outside diameter of membrane
d_{lm}	Logarithmic mean diameters of the membrane fiber
EDA	Ethylenediamine
ePTFE	Expanded polytetrafluoroethylene
Fe_3O_4	Ferrous ferric oxide
GAM	Gas absorption membrane
GFR	Gas flow rate
HFM	Hollow fiber membrane
HFMCS	Hollow fiber membrane contactors
H_2S	Hydrogen sulfide
K_{OG}	Gas phase overall mass transfer coefficient
K_{OL}	Liquid phase overall mass transfer coefficient
K_{G}	Individual mass transfer coefficient of gas
K_{L}	Individual mass transfer coefficient of liquid
K_{M}	Individual mass transfer coefficient of membrane

K_2CO_3	Potassium carbonate
KOH	Potassium hydroxide
LFR	Liquid flow rate
M	Molarity
m	Henry's constant
MEA	Ethanolamine
MTC	Mass transfer coefficient
N_2	Nitrogen
NaOH	Sodium hydroxide
OD	Outside diameter
PE	Polyethylene
PES	Polyethersulfone
PFA	Poly tetrafluoroethylene-co-perfluorinated alkyl vinyl ether
PP	Polypropylene
PS	Polysulfone
PTFE	Polytetrafluoroethylene
PVDF	Poly(vinylidene fluoride)
RG	Mass transfer resistance in gas
RL	Mass transfer resistance in liquid
RM	Mass transfer resistance in membrane
ROG	Overall mass transfer resistance
SEM	Scanning Electron Microscope
SiO_2	Silicon dioxide
TEA	Triethanolamine

Chapter 1: Introduction

1.1 Overview

A well-developed strategy called Carbon Capture and Storage (CCS) has been used to control the significant CO₂ emission. It's defined as a process of separating CO₂, transporting and storing it in isolated locations (Cambridge University press, 2005). CO₂ Separation stage covers the highest energy consumption (75-80% of total cost) (Davison, 2007). To accomplish CCS strategy, several separation techniques have been adopted; adsorption, physical and chemical absorption and cryogenic separation. The previous technologies showed valuable performance in terms of removing CO₂ but still facing serious drawbacks that forced researchers to explore adjusted techniques.

One modified technique has been used as an alternative to the CO₂ separation techniques which is membrane contactors. This technology covered several advantages compared to the conventional techniques. They can provide 20 to 100 times more surface area per unit volume and avoid some operational problems such as entrainment. Added to previous, membrane contactors allows even smaller flow rates compared to flow rates used in packed bed towers.

The uses of membrane contactors in separations processes involve gas separations or liquid-liquid extractions. For gas separations processes, the most well-known membranes used are the hollow fiber membranes where it shows a promising way to enhance the gas separation processes. Such advantages can be observed through the flexibility of operating the system, the ease of scale-up and the reduction in energy consumption (Al-saffar, Ozturk, & Hughes, 1997).

1.2 Statement of the problem

The high demand on natural gas in UAE encouraged researchers to concentrate on offering several methods to treat natural gas before using it. Treating natural gas means removing undesirable contaminants such as acid gases (carbon dioxide and hydrogen sulfide) from the gas mixture before liquefying it. The acid gases are toxic and may cause corrosion to gas pipelines. For that purpose, plenty of researchers have been examining the most appropriate method to remove acid gases.

A proposed technology to separate CO₂ from gas mixture was studied and optimized to enhance the CO₂ removal efficiency. The process called “Gas Absorption Membrane Contactors” where acid gases are being captured and separated from gas mixture using physical or chemical solvent.

In this study, the focusing was on removing carbon dioxide from synthetic gas mixture (5% CO₂ and 95% CH₄) using chemical solvent (sodium hydroxide). The investigation targeted the performance of gas absorption membrane contactors operated at high-pressure and packed with glass beads. The purpose of using beads is to help in increasing the turbulence in the solvent, with the aim to enhance the removal efficiency. Additionally, it allows more contact between the targeted gas (CO₂) and the absorbent solvent. Operating at high pressure was studied to generate results similar to the industrial operating conditions (high pressure). The hollow fiber membranes used was poly tetrafluoroethylene-co-perfluorinated alkyl vinyl ether (PFA).

1.3 Research objectives

The main objectives of this work are listed below:

- 1- Fabricate high-pressure hollow fiber membrane contactors (HFMCs) for CO₂ absorption using poly (tetrafluoroethylene-co-perfluorinated alkylvinyl ether (PFA).
- 2- Investigate experimentally the mass transfer of CO₂ through membrane contactors packed with glass beads under high pressure and compare the results with these of non-packed contactors.
- 3- Investigate the effect of the operating parameters such as the liquid/gas flow rates, amine type, pressure, the concentration of inlet solvent stream and beads size.
- 4- Calculate the mass transfer coefficient from theoretical model and compare with those obtained from experimental results.

1.4 Limitations of the Study

Although the experimental work was done successfully, there were some limitations faced during the experiment. Fabrication of modules was the most time-consuming step in this work. It took a long period of time to prove its reliability in conducting an experiment.

1.5 Organization of the thesis

The outline of this work will be covering: Chapter1 will cover a brief overview of techniques used in capturing carbon dioxide, the problem statement of current work, the research objectives and some limitations faced. Chapter 2 will introduce the conventional techniques in capturing carbon dioxide, the alternative technique which is “Gas Membrane Absorption” (GAM), some recent work done by researchers worldwide, the characteristics of membrane fiber and its compatibility with absorbent. The fabrication of hollow fiber membrane contactors and the experimental setup will be discussed in Chapter 3. In Chapter 4, the experimental results will be presented (in terms of tables and figures) and explained simultaneously. Eventually, Chapter 5 will summarize the findings and suggested recommendations.

Chapter 2: Relevant Literature

2.1 Conventional gas separation techniques

Several conventional techniques have been associated with the removal of acid gases for environmental and economic goals such as; absorption, adsorption, chemical looping combustion, membrane separation, hydrate-based separation and cryogenic distillation (Leung, Caramanna, & Maroto-Valer, 2014). Among these techniques two separation processes will be discussed; Absorption and Membrane separation.

Absorption consists of two columns; absorption column where the acid gases are being separated from raw gas and stripping column where the solvent is being regenerated. Absorption can be classified according to the solvent used; physical absorption where the solvent absorbs acid gases whereas in the chemical absorption the acid gases are being absorbed and reacted with the solvent. Chemical absorption is the most mature process used in industry. Common chemical solvents used in this process; primary amines like monoethanolamine (MEA), secondary amines such as diethanolamine (DEA), triethanolamine (TEA) which is called tertiary amines and potassium carbonate (K_2CO_3). Among these solvents, the most adapted solvent is MEA that is known for its high removal efficiency (> 90%), economical and commercially available. At the same time, it showed some drawbacks like energy consumption, absorbent degradation, and corrosion. Figure 1 shows the general schematic diagram for CO_2 absorption process (Songolzadeh, Soleimani, Takht Ravanchi, & Songolzadeh, 2014).

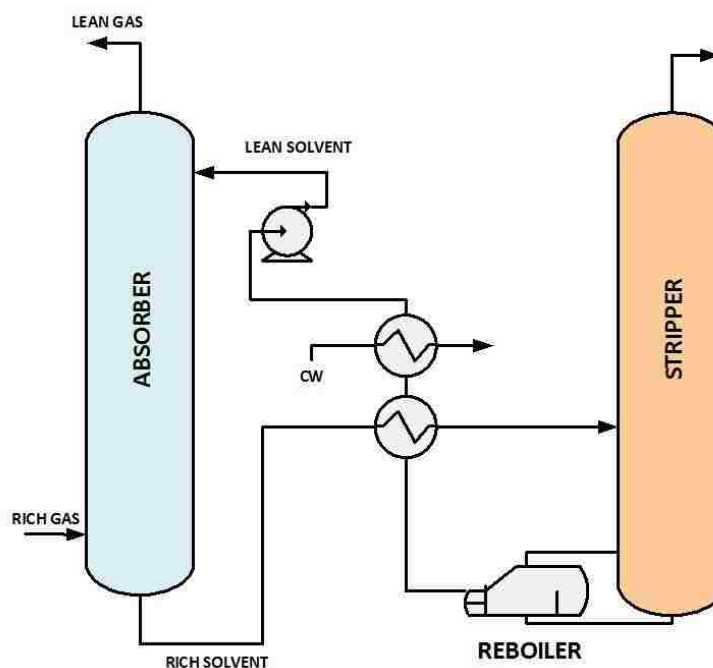


Figure 1: Schematic diagram of CO₂ absorption plant

The other conventional technique is membrane separation where it can be accomplished by species permeability or solvent selectivity. The permeation technique depends on the pressure difference between the membrane sides where the targeted molecules permeate through small pores. On the other hand, larger pores are the characteristics of the selectivity process where different sizes of molecules penetrate through the pores to meet the solvent that will select and absorb the targeted molecules. The low purity and low feed acid gas concentration are the limitations surrounded by membrane separation processes. Addition to that, the possibility of damaging the membrane by elevated operating conditions (high temperature) or existing chemicals in the gas mixtures are high (Brunetti, Scura, Barbieri, & Drioli, 2010).

2.2 Potential candidate for gas separation-Gas absorption membrane (GAM)

An alternative technology which is the gas absorption membrane (GAM) is used as CO₂ separation where the gas is being exposed to chemical solvent in order to remove the acid gases. It is considered to be a combination of absorption and membrane separation. The compactness played a major role in considering the gas absorption membrane unit as one of the most sustainable technique in gas separation (Qi & Cussler, 1985). The heat exchanger concept used to allow the independent control of gas and liquid flow rates (Rezaei, Ismail, Hashemifard, & Matsuura, 2014). The microporous membrane in this system functions as a mass transfer medium instead of the separation medium. The presence of microporous membrane allows indirect contact between the gases and the solvent which in turn reduces the operational problems such as flooding, channeling and foaming (Qi & Cussler, 1985). Another advantage of using GAM is the high efficiency and reduction in required energy (Songolzadeh et al., 2014). Addition to that, GAM offers a high interfacial area per unit volume and easy scaling up. The ability to combine two processes (absorption and membrane) enables higher removal compared to the conventional methods.

In the meanwhile, the process showed some weaknesses such as the additional resistance caused by the presence of membrane fibers. To overcome this issue, researchers suggested decreasing the membrane thickness or increasing the membrane porosity (D. Wang, Li, & Teo, 2000). Another concern has been investigated when using gas absorption membrane process is the wetting problem where the membrane gets wet by the absorbent liquid for a long time (Mavroudi, Kaldis, & Sakellaropoulos, 2003). (B.-S. Kim & Harriott, 1987) suggested increasing the absorbent pressure not to be exceeding the breakthrough pressure to avoid any membrane wetting. Moreover,

the non-uniform fiber distribution is another disadvantage in gas absorption membrane process which can lead to channeling problems. Besides the module geometry and membrane structure, the operating conditions play a major role in the performance of hollow fiber membrane contactors. Increasing the solvent temperature increases the reaction rate of chemical absorption. At the same time, it decreases the liquid surface tension and solubility, wets the membrane and changes the membrane properties.

2.2.1 Membrane gas separation at high pressure

Researchers have been investigating the performance of HFMCs for different applications. Starting with (Bothun et al., 2003) where the feasibility of extracting aqueous solutes using HFMCs at high pressure was studied. The results showed a favorable performance of polypropylene HFM in terms of extracting ethanol and acetone. Another study done by (Dindore, Brilman, Feron, & Versteeg, 2004) examined the efficiency of operating at elevated pressure (up to 20 bars) when using single hollow fiber membrane contactor. Polypropylene hollow fiber membrane was used as a porous barrier between the gas mixture (CO_2 and N_2) and the chemical solvent (propylene carbonate). The outcomes showed an increase in CO_2 pressure results in higher rates of removal.

Marzouk and his team (Marzouk et al., 2010) have designed and constructed hollow fiber membrane modules for the purpose of operating at high pressure. The modules were constructed from a stainless steel material and filled with expanded polytetrafluoroethylene (ePTFE) hollow fibers. Different solvents (distilled water, aqueous sodium hydroxide, and different amine solutions) were used to investigate the removal efficiency of CO_2 at high pressure. The experimental data proved the benefit of increasing the pressure in increasing the CO_2 flux. The previous investigations were

focusing on low CO₂ concentration (<20%) in the feed. Additional study on the performance of hollow fiber membrane contactors was done by (Kang, Chan, Saleh, & Cao, 2017) but for concentrated gas feed (45% and 70% of CO₂). The experimental materials consist of poly(vinylidene fluoride) (PVDF) as the hollow fiber membrane and the activated MDEA (aMDEA) with piperazine as the chemical solvent. In terms of %CO₂ removal efficiency, the results showed 33.3 % enhancement at 1 bar and 91.3% enhancement at 60 bar.

2.2.2 Packed membrane gas contactors

Other researchers aim was to enhance the hollow fiber membrane system by applying the nanotechnology in their studies. The enhancement of the system was accomplished by adding nanofluids to act as an absorbent. Nanofluids are defined as solvent filled with nanometer material (nanofibers, nanoparticles, nanorods, nanosheet, nanowires, nanotubes, or droplets). Choi was the first recommended the beneficial use of nanofluids (Choi & Eastman, 1995). Researchers proved its ability to enhance the thermal diffusivity and conductivity, viscosity and convective heat transfer coefficient compared to normal fluids (Verma & Tiwari, 2017). Back in the nineteenth the nanofluids concept was used by lots of researchers in gas separation field and the results showed improvement in the removal of some gases (SO₂ and O₂). Further studies were conducted to investigate the CO₂ absorption using membrane gas absorption process and nanofluids as a solvent.

Starting with the work done by Golkhar (Golkhar, Keshavarz, & Mowla, 2013); where their paper discussed the uses of nanoparticles (nanosilica) and carbon nanotube as an absorbent in enhancing the removal of CO₂. The nanosilica particles or carbon nanotube were fed to the tube side separately and a mixture of air and CO₂ was fed co-

currently to the shell side. The result showed some improvement in the removal efficiency of CO₂ by both nanosilica and carbon nanotube.

Another paper discussed the uses of nanoparticles where different types of nanoparticles (Fe₃O₄, CNT, SiO₂, and Al₂O₃) were injected in the contactor, distilled water carrying the nanoparticles was fed to the tube side of the contactor and the gas was fed co-currently to shell side. The results indicated the progressive effect of the presence of particles on the absorption of CO₂ (Peyravi, Keshavarz, & Mowla, 2015). A 2D mathematical model developed by (Darabi, Rahimi, & Molaei Dehkordi, 2017) for CO₂ absorption using nanoparticles was validated by the experimental results reported by (Peyravi et al., 2015). A recent study on nanofluids was conducted by (Mohammaddoost, Azari, Ansarpour, & Osfouri, 2018) where the polypropylene fiber membranes were used to separate CO₂ from gas mixture (40% CO₂ and 60% N₂) using metal oxide nanoparticles (NPs) like aluminum oxide (Al₂O₃), titanium dioxide (TiO₂) and silica (SiO₂). The results confirmed 98.9% CO₂ removal obtained by Al₂O₃ nanoparticles.

2.3 Membrane characteristics

For the purpose of selecting suitable microporous membrane for CO₂ removal, some characteristics needed to be considered. An ideal microporous membrane is fabricated from hydrophobic polymer material of high porosity and small thickness of 10-300 μm and pore size of 0.1 – 1 μm (Mansourizadeh & Ismail, 2009). Table 1 summarizes the characteristics of some membrane fibers used in gas absorption membrane contactors.

Table 1: Characteristics of selected hollow fiber membranes

Membrane	ID (μm)	OD (μm)	Thickness (μm)	Pore size (μm)	Porosity (%)	Reference
Polysulfone (PS)	200	400	100	0.05		(Ren et al., 2006)
Polyethersulfone (PES)	460	850	195	-	-	(K. Li & Teo, 1998)
Polyethylene (PE)	482	706	112	-	0.82	(Nishikawa et al., 1995)
Polytetrafluoroethylene (PTFE)	1000	1700	350	-	0.40	(Nishikawa et al., 1995)
Poly(vinylidene fluoride) (PVDF)	300	514	107	-	0.698	(Atchariyawut, Feng, Wang, Jiraratananon, & Liang, 2006)
(ePTFE)	100	200	50	-	18.1	(Marzouk, Al- Marzouqi, Teramoto, Abdullatif, & Ismail, 2012)

As seen from Table 1, the pore size measurement is rarely reported but it can be measured using Scanning Electron Microscope (SEM).

2.4 Membrane absorbent compatibility

As reported by (Faiz & Al-Marzouqi, 2010; Feng, Wang, Zhang, & Shi, 2011; Khaisri, deMontigny, Tontiwachwuthikul, & Jiraratananon, 2009) the compatibility between the solvent, the membrane, and the gas affects the removal efficiency of CO₂. For that reason, researchers investigated the compatibility of membrane and absorbent by immersing different membranes fibers in different solvents for a period of time. Table 2 shows the experimental results (deMontigny, Tontiwachwuthikul, & Chakma, 2006).

Table 2: Membrane-absorbent compatibility

Solvent	PTFE	PP	PVDF	PES	PS
Water	Yes	Yes	Yes	Yes	Yes
Propylene carbonate	Yes	Yes	No	No	No
Selexol	Yes	No	No	No	No
N-methyl pyrrolidone	No	No	No	No	No
Dimethyl formamide	No	No	No	No	No
Tributyl phosphate	No	No	No	No	No
Glycerol triacetate	Yes	No	No	No	No
N-formyl morpholine	Yes	Yes	No	No	No

2.5 Membrane wetting

Membrane wetting generally occurs when the pressure difference of liquid is higher than the breakthrough pressure. In that case, the liquid will penetrate into the pores of the membranes. For that reason, the breakthrough pressure must be measured

to avoid any wetting. The breakthrough pressure can be measured by Laplace-Young equation which describes the maximum pressure difference that can be measured to prevent any wetting in the system (B.-S. Kim & Harriott, 1987).

$$\Delta p = \frac{2\gamma \cos \theta}{r_{p,max}} \quad \text{Equation 1}$$

Where γ is the liquid surface tension, θ is contact angle between the fluid phase and membrane and $r_{p,max}$ is the maximum membrane pore radius.

Although Laplace-Young equation showed reliable results in measuring the breakthrough pressure, there are still some difficulties to obtain accurate measurements due to several factors; the non-uniform pore size of membrane fibers and the countercurrent flow direction can cause inconsistent measurements of breakthrough pressure (Dindore et al., 2004). Moreover, some liquids (ionic species, complexes, and impurities) can change the morphology of membrane because of their high concentrations or low surface tension (Zha, Fane, Fell, & Schofield, 1992).

Another suggestions by (J.-L. Li & Chen, 2005) were listed to avoid membrane wettability:

1. Operating at a pressure less than the breakthrough pressure.
2. Using hydrophobic membranes to increase the contact angle between the membrane and solvent used.
3. Surface modification of membrane by coating the membrane with a thin permeable layer (Dickson, Childs, McCarry, & Gagnon, 1998), surface grafting (Xu, Wang, Shen, Men, & Xu, 2002), pore filling grafting (Mika,

Childs, Dickson, McCarry, & Gagnon, 1995) or in-situ polymerization (Gabriel & Gillberg, 1993).

4. Using composite membrane; consist of the upper layer that is highly permeable and hydrophobic to be in contact with liquid which provides stabilization for the membrane (Nymeijer, Folkers, Breebaart, Mulder, & Wessling, 2004).
5. Controlling and optimizing operating conditions; especially the liquid pressure. (K. Li & Teo, 1998) suggested keeping the liquid pressure higher than the gas pressure to avoid any membrane wettability and forming bubbles.

2.6 Membrane mass transfer coefficient

Mass transfer coefficient analysis is being used in the interest of evaluating the gas absorption into the liquid through a microporous membrane. Two schemes were suggested; gas flows in the lumen side and diffuses through membrane to reach the pore mouth where it dissolves and reacts with liquid which flows in the shell side. The other scheme is the opposite where gas flows in shell side and meets the liquid in tube side. Several publications described both scenarios for different membrane fibers and solvents. For the gas flowing in the tube side, the overall mass transfer coefficient was studied by (Jin et al., 2017) for simultaneous removal of CO₂ and H₂S using physical absorption (water) and chemical absorption (MEA, K₂CO₃, KOH, PS). The hollow fiber membrane used was Poly (vinylidene fluoride) (PVDF). For H₂S gas; when increasing the gas flow rate, the mass transfer resistance increased and the major mass transfer resistance occurred in the gas phase. This was explained by the improvement of hydrodynamics of gas inside the fibers. Similar results were found by other researchers (D. Wang, Teo, & Li, 2002); (Hedayat, Soltanieh, & Mousavi, 2011). On

the other hand, removal CO_2 showed noticeable mass transfer resistance in the liquid phase when increasing the liquid flow rate. The number of molecules of CO_2 at the interface is larger than number of molecules in H_2S as explained by low reaction rate constant between CO_2 and solvent used (MEA).

Another study was done by (Mavroudi et al., 2003) where a mixture of CO_2 and N_2 was exposed to a Liqui-Cel Extra Flow membrane contactor. The solvent used was water and diethanolamine (DEA). The results demonstrated a comparison between the theoretical and experimental model for MTC and concluded the presence of wetting during the experiment. Moreover, to evaluate the second scenario, (Marzouk et al., 2012) examined the simultaneous removal of H_2S and CO_2 at elevated pressure using expanded poly(tetrafluoroethylene) (ePTFE) and poly(tetrafluoroethylene-co-perfluorinated alkylvinyl ether) (PFA). Their experimental results were in agreement with the theoretical model for physical absorption.

The previous publications described the gas phase overall mass transfer coefficient (K_{OG}). Other researchers were interested in the liquid phase overall mass transfer coefficient (K_{OL}). (Atcharyawut et al., 2006) studied the effect of (PVDF) membrane structure on the mass transfer resistance for physical absorption. Moreover, (Atcharyawut, Jiratananon, & Wang, 2007) studied the liquid overall mass transfer coefficient for PVDF microporous membrane for physical and chemical absorption. The results showed higher overall mass transfer coefficient for chemical absorption compared to physical one.

Chapter 3: Experimental Work

3.1 Construction and preparation of hollow fiber membrane contactors

The construction process went through two main stages; mechanical part and chemical part. The mechanical part accounted for the manufacturing of the acrylic tubes, disks, and filters whereas the chemical part included the pretreatment of fibers.

3.1.1 The mechanical part

The mechanical part consists of manufacturing four main parts; acrylic tube, acrylic disks, filter and acrylic covers. Selecting the acrylic material was because of its ability to stand high pressure (> 25 bars) and ease of tracing the flow pattern in the module since it is a transparent material. The acrylic material had two configurations; acrylic tubes and acrylic sheet. The acrylic tubes and sheets had large thickness (5 mm and 300 mm respectively) to operate at elevated pressure with no concerns. Some researchers relied on using acrylic in their experiment such as (Cui & deMontigny, 2017) since it showed chemical compatibility with alkanolamine solutions.

Acrylic tube

The commercial acrylic tubes (30 mm OD, 20 mm ID and 5 mm thickness) were cut into tubes of 30 cm length. The inner wall of the tube was threaded to enhance the bonding between fibers and tube. Cutting the acrylic tube was not possible in the laboratory due to the lack of cutting instrument. Each tube was shielded with circular acrylic disks for safety concerns.

Acrylic disks

A commercial flat sheet of acrylic was cut into disks of 3 cm thickness and a diameter of 8 cm. Moreover, each disk had 3 main holes for screws to join the disks together. Each side of the tube had two disks and supported by a cover disk. Several holes were drilled on these disks. The first disk had one hole bonded by 6mm stainless steel discharger tube considered as the entrance and exit of shell side. Drilling this hole went through two sizes; 6mm hole to add the stainless steel discharger and 12 mm hole to add a portion of the commercial epoxy. The second disk had two holes bonded by 3mm stainless steel stoppers to increase the welding of disks to the tube. Additional hole was drilled to inject epoxy for welding purposes. All these disks were welded to the acrylic tube by Trichloromethane solvent. Figure 2 shows the acrylic disks and their specifications.

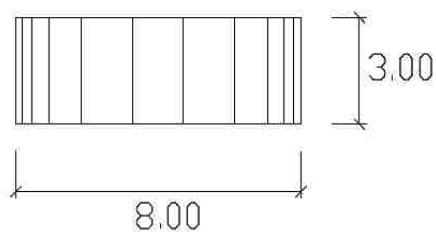
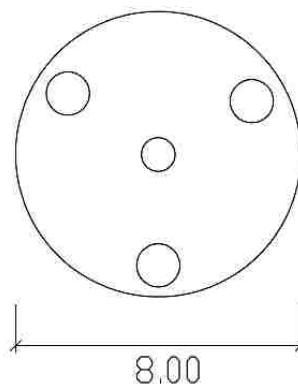


Figure 2: Disk structure

Cover disks

The cover disks were drilled to assemble 6mm discharger stainless steel tube. These stainless steel tubes present the entrance and exit of tube flow. The back side of the disk was covered with 4mm thickness O-rings to increase the soldering between the cover disks and the tube. Figure 3 shows the specifications of cover disks fabricated.

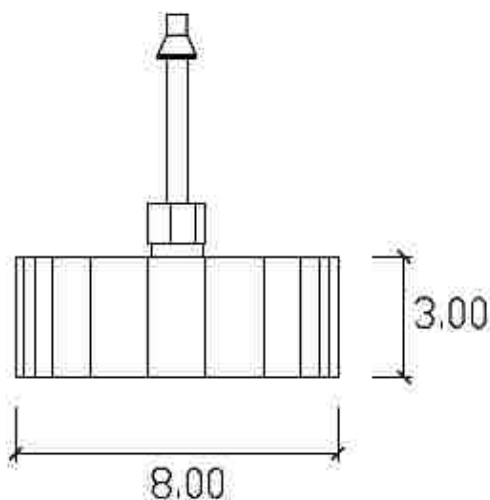
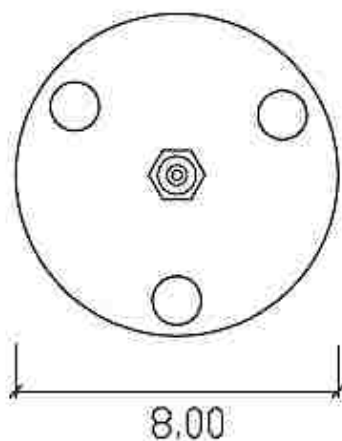


Figure 3: Cover disk structure

Filter

A transparent filter was fabricated to ensure the beads used are not being transferred to the other side of the shell. The same acrylic sheet used in cutting disks was cut into smaller diameters and bonded to stainless steel discharger as an inlet and outlet of the filter. In between, a porous membrane was added to inhibit the flow of beads. Figure 4 shows the filter structure.

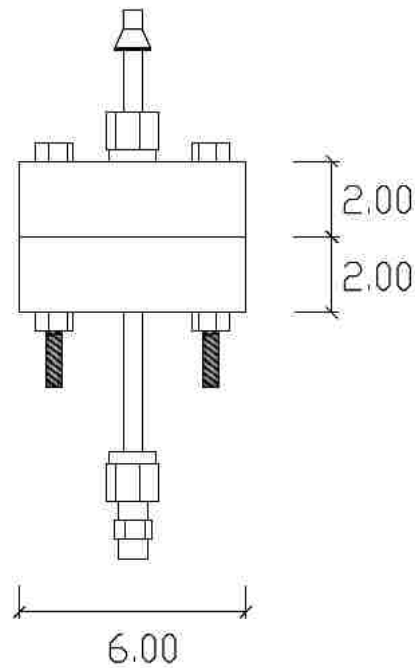


Figure 4: Filter structure

3.1.2 The chemical part

The preparation of fibers was initially started by the etching process. The aim of etching is to increase the roughness of fiber surface and enhance the bonding between the acrylic tube and the fibers. A sodium-based etching solution was used to etch the ends of the fiber and leave an active part (in the middle) without etching. The length of the active part was 18 cm. The etched parts then were washed with distilled water then cleaned with ethyl alcohol.

Around 11-gram portion of paste type epoxy (EpoPutty) was used on the ends of fibers to center them in the tube. The epoxy was kept for 1 h to ensure proper curing. The EpoPutty was also used to cover all holes drilled for safety concerns. A commercial epoxy consists of two-part low-viscosity (Buehler) was used for further bonding between the fibers and the tube. The two parts were mixed according to the manufacturer recommendation and then injected through the hole in the second disks

to ensure all air bubbles are escaped from the top. The module was positioned vertically to get benefit from the gravity force when injecting and make sure the epoxy penetrate and fill the spaces between the fibers and the threaded cavities of the tube inner wall. Each side of the tube took 24 h to reach the curing and guarantee long operational lifetime.

For module packed with beads, three different sizes of beads were used; 0.25, 1 and 2 mm. Table 3 shows the amount used for each size.

Table 3: The number of beads used for each size

Size (<i>mm</i>)	Amount (<i>g</i>)
0.25	100
1	65
2	40

The same procedure was followed for module without beads. The only difference between them is adding the beads before injecting epoxy into the second side of the tube. Figure 5 and Figure 6 show the completed module structure drawings.

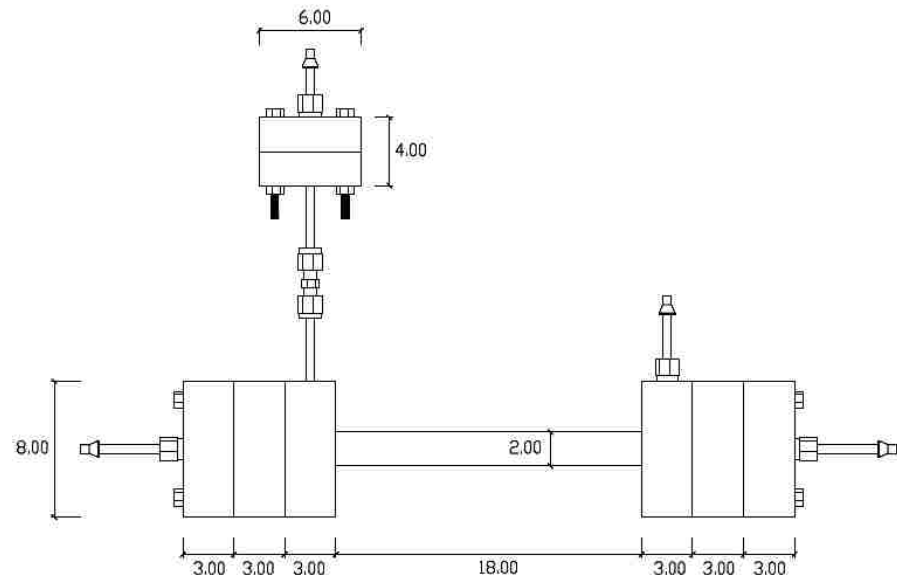


Figure 5: Module structure drawing

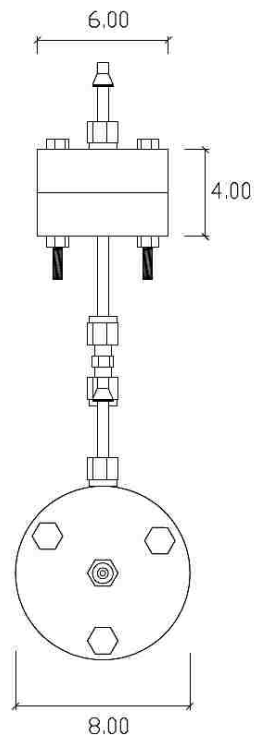


Figure 6: Front side of the module

3.2 Experimental set-up

The experimental setup was already fixed at the laboratory in UAE University. A custom designed heavy-walled plexiglass safety compartment (MI, USA) was used to ensure safe environment while working at high pressure. Inside the compartment, all experimental apparatuses were housed there and Figure 7 shows the schematic diagram of the experimental setup.

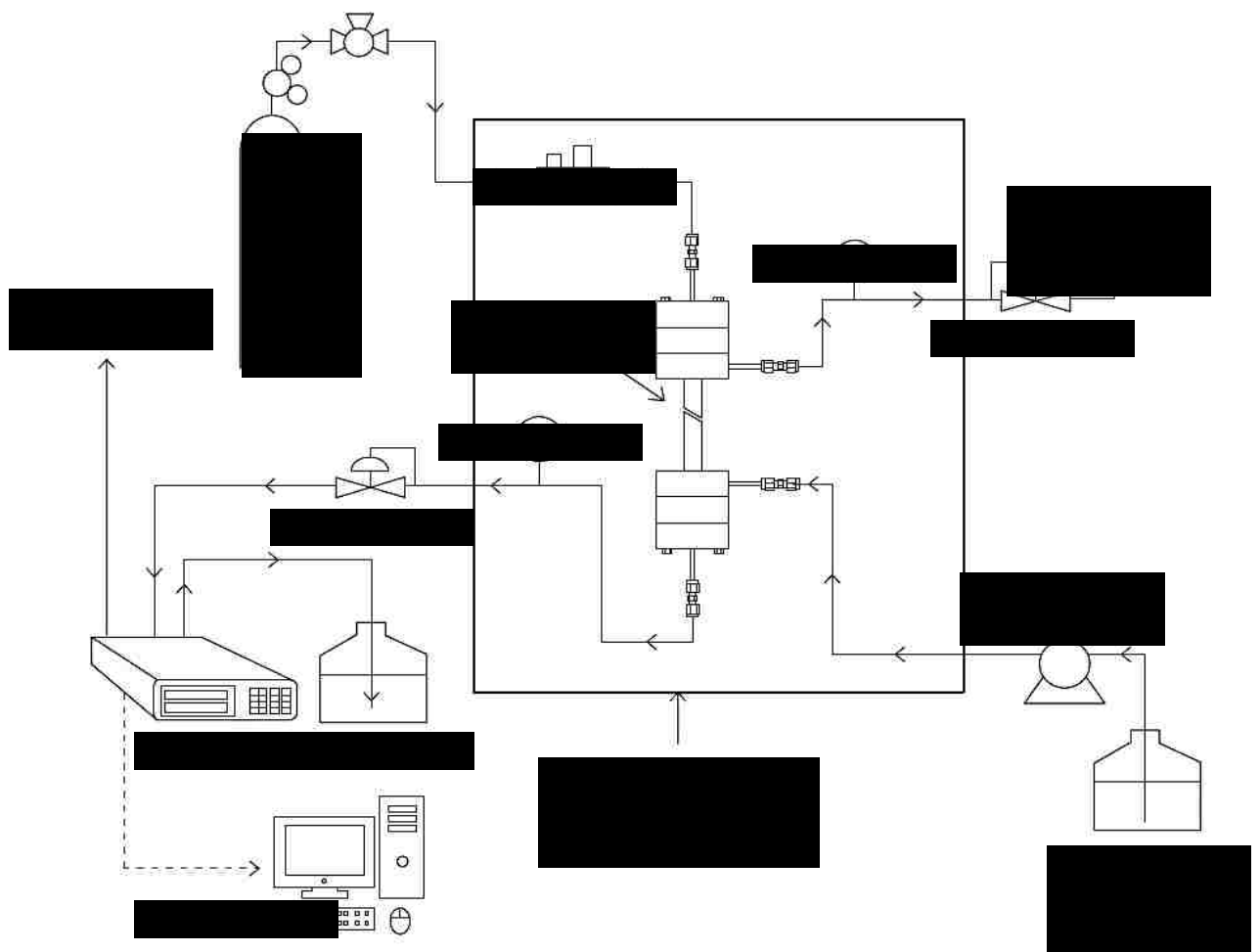


Figure 7: Experimental setup used for CO₂ removal at elevated pressure

The gas flow rate was set by a mass flow controller (Parker, Porter model 201) and fed to the system through the tube side and controlled by a back pressure regulator (Tescom). At the same time, the solvent was pumped to the shell side by a high-pressure pump (Knauer pneumatic pump, max flow 499.9 mL/min and max pressure 100 bar) and also controlled by a back pressure regulator (Tescom). Both feed pressures (gas and solvent) were monitored using High-pressure digital gauges (Cole Parmer). To avoid any wetting, the solvent pressure was kept higher than the gas feed pressure by approximately 0.5 bars. The outlet gas stream was fed to the 2-channel CO₂/CH₄ infrared analyzer (California Analytical Instruments) to observe the change in the concentration of mixture (CO₂ and CH₄). This data was recorded by data acquisition interface card (Pico Tech.) and saved in a PC installed with PicoLog software (Pico Tech.).

Chapter 4: Results and Discussion

The main objectives of this work include: (1) design and fabricate a custom-made HFMCs using transparent acrylic material and can be used at elevated pressures (up to 25 bars), (2) to investigate the effect of packing HFMCs with glass beads on %CO₂ removal efficiency, and (3) compare the overall mass transfer coefficient obtained from experimental data with those of the modeling.

4.1 Construction and fabrication of custom-made HFMCs

Beneficial to select the appropriate design for the investigation, several parameters were studied to come up with the most suitable design. The following sections explain how each part of the construction was chosen.

4.1.1 Selection of membrane

As discussed in the section 2.5, several characteristics need to be fulfilled when selecting the membrane type such as the hydrophobicity of the membrane, the porosity and the pore size, the thickness of the membrane and its stability.

Generally, hydrophobic membranes are extensively used in gas separation due to their high contact angle compared to hydrophilic membranes. Other factors to be considered are pore size, long-term stability, and compatibility with an absorbent (Zhang et al., 2014). Based on these factors, the fiber membrane selected was Poly(tetrafluoroethylene-co-perfluoro-(propyl vinyl ether) (PFA) which showed high compatibility with alkanolamine solutions, good mechanical properties, high hydrophobicity, long stability among others. As reported by Al Marzouqi (Al-Marzouqi, Marzouk, & Abdullatif, 2017) PFA membrane stability was investigated

based on industrial conditions (high pressure and temperature) for the first time. The synthetic gas contained several compositions of natural gas (Methane 81.64%, Ethane 6.9%, Propane 3.6%, I-butane 0.3%, N-Butane 0.56%, Carbon dioxide 4.2%, Hydrogen Sulfide 1.4%, and Nitrogen 1.4%) and it was fed to the shell side at elevated temperature and pressure (50 °C and 50 bar respectively). On the other side of hollow fiber membrane contactor, a chemical solvent consists of 30 wt % K_2CO_3 , 1 wt % DEA was fed counter currently to the tube side at a temperature of 100 °C and pressure of 50 bars. The experiment was conducted 6-8 h per day for 36 working days. The result showed reliable flux values of CO_2 and H_2S removal and there were no signs of any membrane wetting.

In order to measure the characteristics of selected membrane, Scanning Electron Microscope (SEM) was used and Figure 8 shows the micrograph taken from SEM.

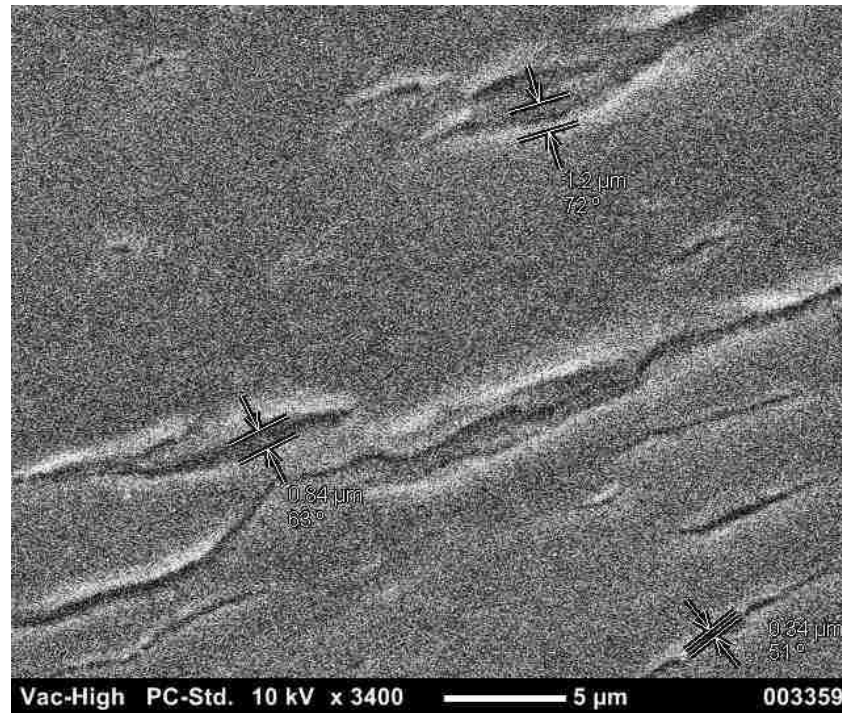


Figure 8: The outer surface of PFA fiber showing the pore diameter.

Table 4 summarizes fiber characteristics for fiber membrane selected (PFA).

Table 4: Membrane characteristics

Fiber type	PFA
OD (μm)	650
ID (μm)	250
Pore size (μm)	0.89
Porosity (%)	56.8

As seen in Figure 8 and Table 4, the PFA membrane have fulfilled the required characteristics for a suitable membrane.

4.1.2 Selection of solvent/gas mixture

Another important factor in gas absorption membrane system is the liquid absorbent. For the sake of selecting appropriate absorbent, several conditions need to be considered. For example, the absorbent should not be toxic or expensive. Also, it should be thermally stable, commercially available and easily regenerated. For long-term operations, the absorbent should not damage the membrane (Mansourizadeh & Ismail, 2009).

The criteria for selecting typical absorbent are governed by several factors:

1. The high reactivity between absorbent and CO₂; to increase the absorption rate and decrease the liquid phase resistances (Yang & Cussler, 1986).
2. Surface tension; ideal absorbent has high surface tension to prevent and membrane wettability (J.-L. Li & Chen, 2005).
3. Chemical compatibility with membrane material is an important factor that determines the long-term stability of membrane (J.-L. Li & Chen, 2005).
4. Low vapor pressure; to avoid membrane wettability caused by filling the membrane pores with vapor (Y. Kim & Lee, 2000).
5. Ease of regeneration; rely on the low heat of reaction with CO₂ (J.-L. Li & Chen, 2005).
6. High thermal stability to ensure the stability of solvent at elevated temperatures and reduce solvent degradation (J.-L. Li & Chen, 2005).
7. High absorption capacity; in which reduces the solvent circulation flow rate required (M. Wang, Lawal, Stephenson, Sidders, & Ramshaw, 2011).
8. Low environmental impact (M. Wang et al., 2011).
9. Low solvent cost and commercially available (M. Wang et al., 2011).

According to (Zhang Z.E., 2014), the arrangement of alkonolamine depending on their high efficiency in removing CO₂ were arranged as follow NaOH>MEA>DEA>TEA. For that reason, NaOH solvent was selected as the main solvent which was involved in most of the experimental work.

The gas mixture was ordered from a local company where it contained 5% CO₂ mixed with 95% CH₄. This synthetic mixture is considered to be similar to the real mixture found in gas fields in UAE (Al-Marzouqi et al., 2017).

4.1.3 Selection of flow direction

Commonly flowing directions are classified into two modes; cross flow and longitudinal flow. For longitudinal flow, it can be in co-current flow or counter-current flow (K. L. Wang & Cussler, 1993). Based on researchers' investigations, the countercurrent mode had the highest CO₂ absorption among other modes (Rajabzadeh, Yoshimoto, Teramoto, Al-Marzouqi, & Matsuyama, 2009). Addition to that, the countercurrent flow offers higher contact area.

In terms of selecting the flow of each fluid; two scenarios were tested; the first scenario is that the gas flows in the shell side whereas liquid flows through tube side. The second scenario is that the gas passes through the lumen side and counter-currently the liquid flows in the shell side. Among these two scenarios, the second one showed better performance compared to the first scenario. The reason behind is that the researchers considered the velocity factor which plays a major role in enhancing the removal of CO₂ from a gas mixture. Usually, it's recommended to allow the gas to spend sufficient time in the module to be absorbed (Al-Marzouqi et al., 2008). Based on calculations the area of the tube and shell side were calculated and it showed a

smaller area in the shell side where the solvent will be flowing. The results were also proven by experiment. Figure 9 and Figure 10 show the custom-made HFMCs.

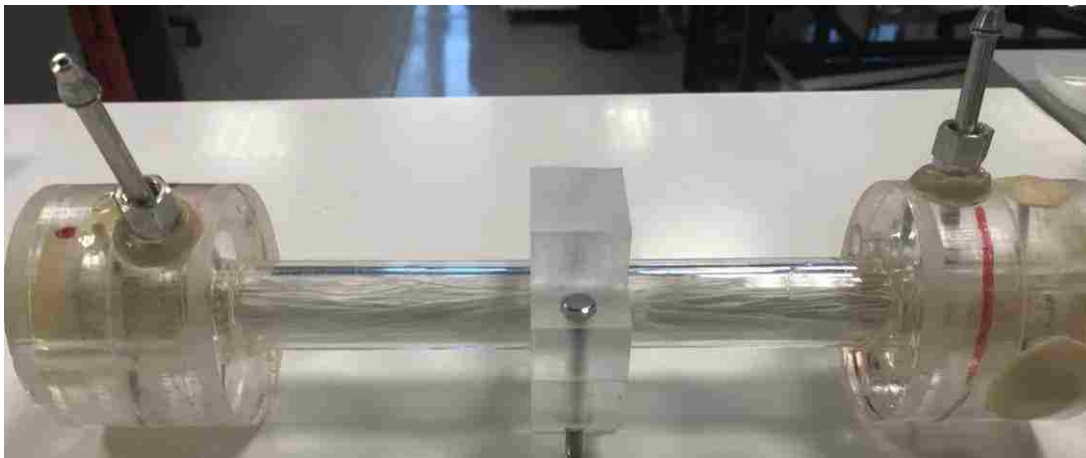


Figure 9: Custom-made HFMCs without glass beads

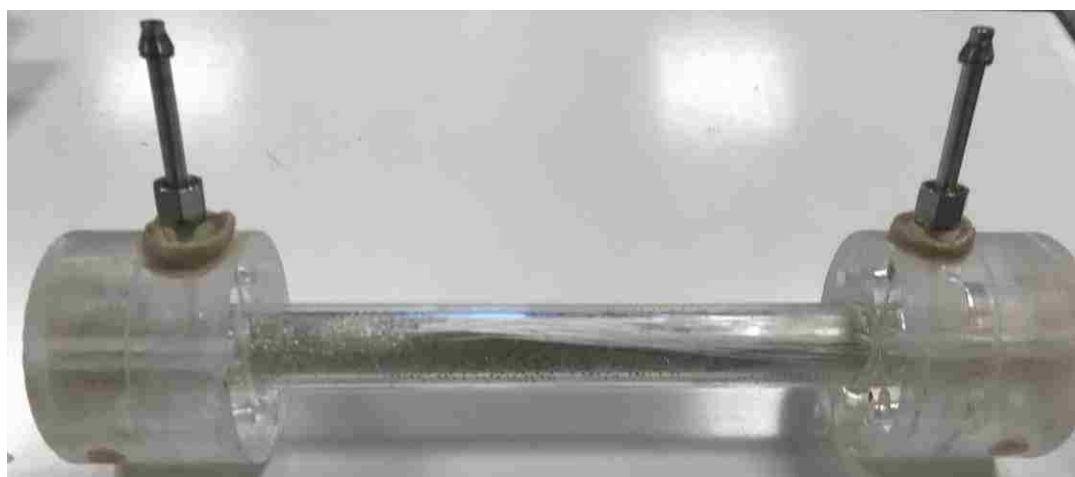


Figure 10: Custom-made HFMCs packed with glass beads

4.2 Experimental investigation of CO₂ removal using PFA fibers

Different operating parameters were studied:

1. The effect of packing HFMCs with beads (diameter of 1 mm).
2. The glass beads size (0.25 mm, 1 mm & 2 mm).
3. Varying gas and liquid flow rates (GFR 1000, 2000 and 3000 mL/min and LFR 10, 20 and 30 mL/min respectively).
4. Different amine used (MEA, DEA, EDA, DETA etc...).
5. The concentration of the inlet solvent (0.25, 0.5 and 1M).

All parameters were tested at different feed gas pressures (up to 25 bars) and ambient temperature for HFMCs using PFA fibers.

4.2.1 Effect of packing HFMCs with beads

For the purpose of simplicity, two letters will be assigned for the two modules; (A) for module without beads and (B) for module packed with beads (diameter of 1 mm). The performance of both modules (A) and (B) in the CO₂ removal was investigated experimentally. Comparison between the two modules was carried out using the gas mixture (5% CO₂ + 95% CH₄) and aqueous sodium hydroxide (1 M) as an absorption solvent. The effect of feed gas pressure on %CO₂ removal and flux was studied at room temperature using fixed gas and liquid flow rates (GFR = 2000 mL/min, LFR = 20 mL/min). The obtained results are presented in Figures 11 and 12.

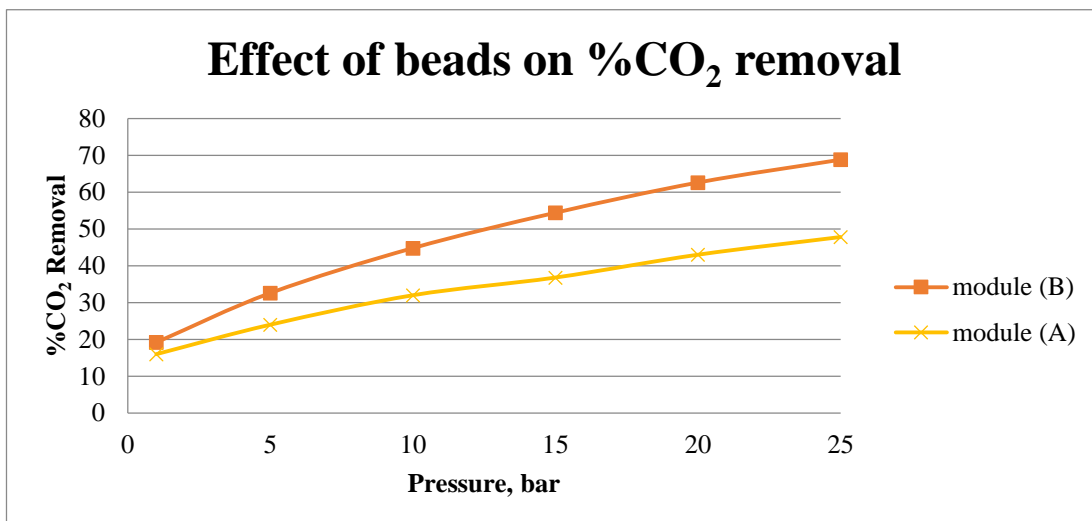


Figure 11: Effect of packing the HFMC with beads (1 mm) on the chemical absorption of %CO₂ using PFA-HFM at fixed gas flow rate (2000 mL/min) and aqueous sodium hydroxide flow rates (20 mL/min).

As stated by Henry's law; the solubility of the gas is function of the pressure. If the pressure increases the molecules are forced to dissolve in the solution which explains the low %CO₂ removal at low pressure and increases as the pressure is increasing for both module (A) and (B) shown in Figure 11. Based on the results, the enhanced removal percentage for module (B) increased from 3% at 1 bar to 21% at 25 bars. This could be attributed to higher solvent velocity in the shell that is packed with beads compared with the one without packing. Moreover, the shell packed with beads enhanced the mixing of the solvent and reduced the liquid resistances as well.

In terms of flux, Figure 12 shows the difference between module (A) and (B).

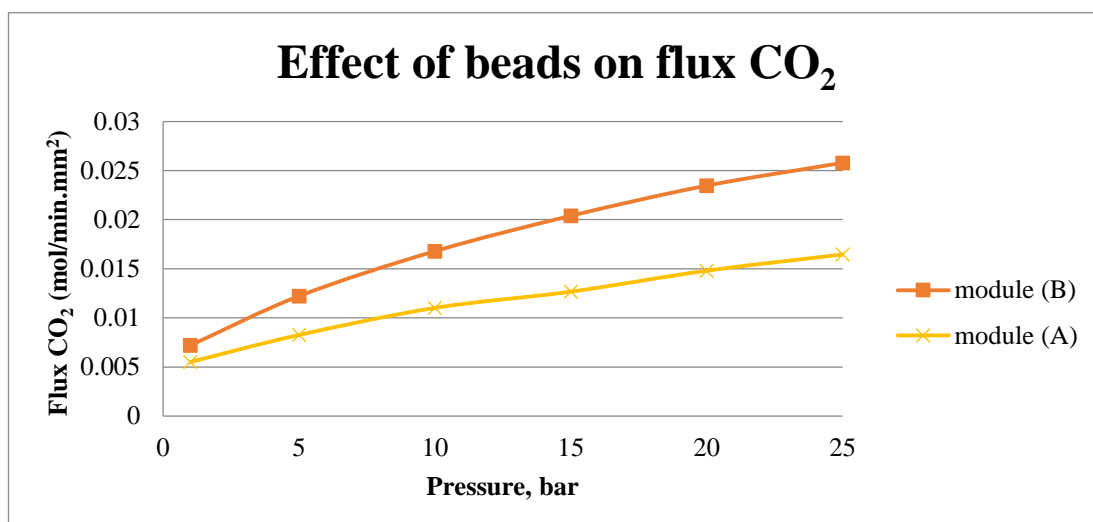


Figure 12: The effect of packing the HFMC with beads (1 mm) in terms of flux using PFA-HFM at fixed gas flow rate (2000 mL/min) and aqueous sodium hydroxide flow rates (20 mL/min).

As seen from Figure 12, at low pressures the solubility had a minor effect on both modules whereas at higher pressures it showed a significant effect on both modules but module (B) had an additional effect which is the presence of beads (as discussed previously).

4.2.2 The effect of glass beads size

Further investigation was conducted to study the effect of beads size on %CO₂ removal efficiency. The absorption solvent used was NaOH (1 M) flowing at a flow rate of 20 mL/min and the gas mixture flow rate was 2000 mL/min, different sizes of bead was tested.

Figure 13 shows the effect of three different sizes of glass beads (0.25 mm, 1 mm and 2 mm) on %CO₂ removal efficiency when compared to the module without beads.

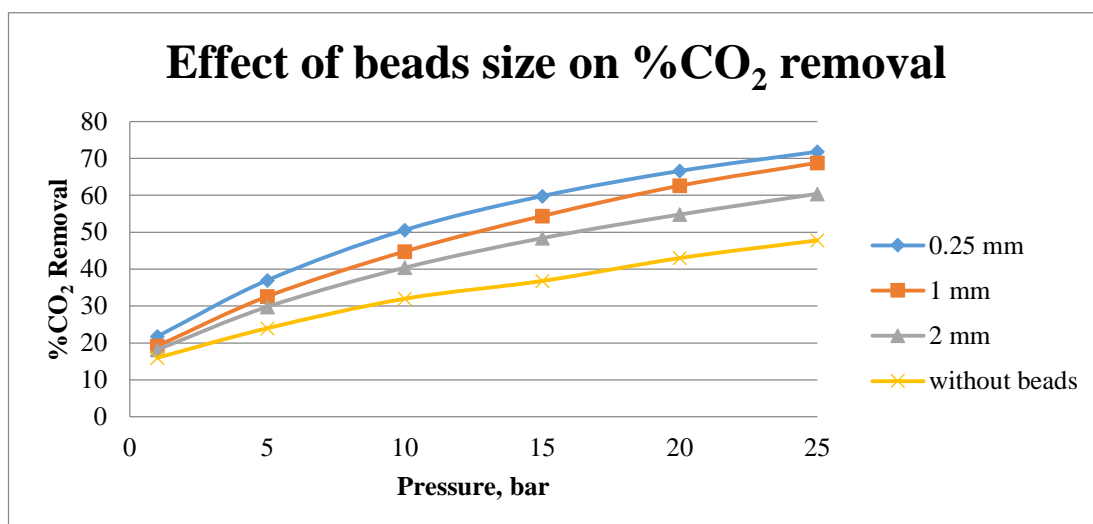


Figure 13: The effect of varying beads size (0.25, 1 and 2 mm) on the chemical absorption of %CO₂ using PFA-HFM at fixed gas flow rate (2000 mL/min) and aqueous sodium hydroxide flow rates (20 mL/min).

The three sizes of beads showed an improvement in %CO₂ removal as compared to the one without beads which can be explained by the turbulences caused by the presence of beads (as mentioned in section 4.2.1). The effect of beads size was studied in terms of velocity where all factors such as gas/liquid flow rates, pressure, and concentration were kept constant and Table 5 shows the calculated velocity for each module.

Table 5: The calculated velocity for each module

Module	Velocity (m/s)
Without beads	1.53E-3
0.25 mm beads	1.55E-2
1 mm beads	4.38E-3
2 mm beads	2.55E-3

Figure 14 shows the results obtained for each module.

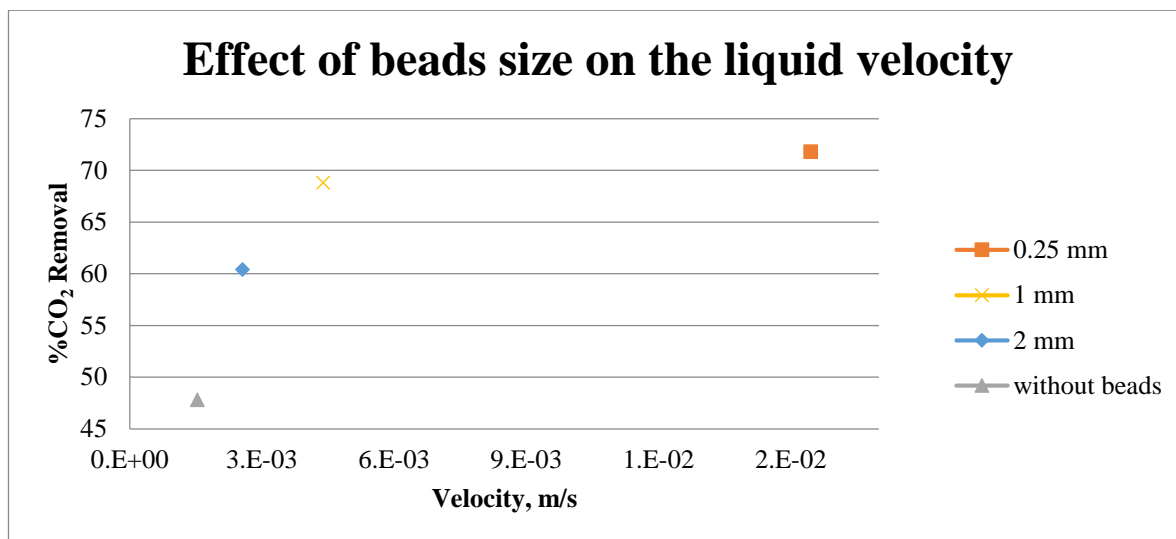


Figure 14: The effect of beads size in terms of velocity using PFA-HFM at fixed gas flow rate (2000 mL/min), aqueous sodium hydroxide flow rates (20 mL/min) and pressure of 15 bars.

As shown in Figure 14; increasing the beads size resulted in decreasing the solvent velocity which in turn reduced the %CO₂ removal. Further explanation will be introduced in section 4.3.3. Addition to that, selecting the glass beads of 1 mm diameter was based on the fact that at pressure of 25 bars, the difference between the glass beads of 2 mm diameter to the 1 mm was about 10% whereas the difference between the 0.25 mm to 1 mm was approximately 2% which is insignificant.

4.2.3 The effect of varying gas flow rate

Different gas flow rates (1000, 2000 and 3000 mL/min) were tested to investigate CO₂ removal efficiency whereas the NaOH (1 M) as an absorption solvent was kept at a flow rate of 20 mL/min. The first part of the investigation was conducted for module (A) and Figure 15 shows the obtained results.

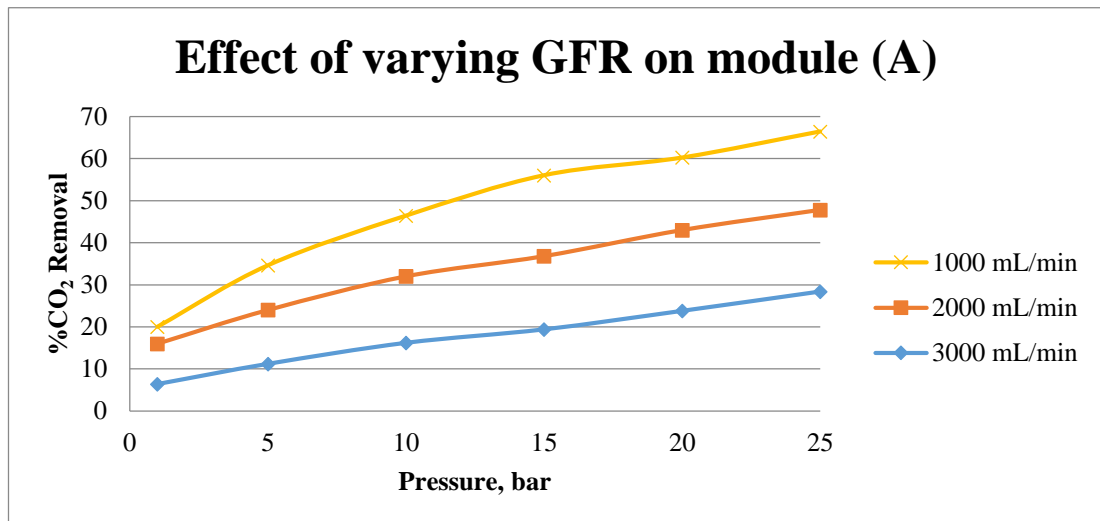


Figure 15: The effect of varying gas flow rate (1000, 2000 and 3000 mL/min) on module (A).

Figure 15 shows an increase in %CO₂ removal by decreasing the gas flow rate which is in agreement with the work done previously by (Marzouk et al., 2010).

Results were explained by the residence time effect where decreasing the flow rate increases the residence time and the %CO₂ removal rate since the gas has more time to spend in the module to be absorbed (Marzouk et al., 2010).

The second part of the investigation was conducted using module (B). The same conditions were used as in the first part of the investigation and the results obtained were shown in Figure 16.

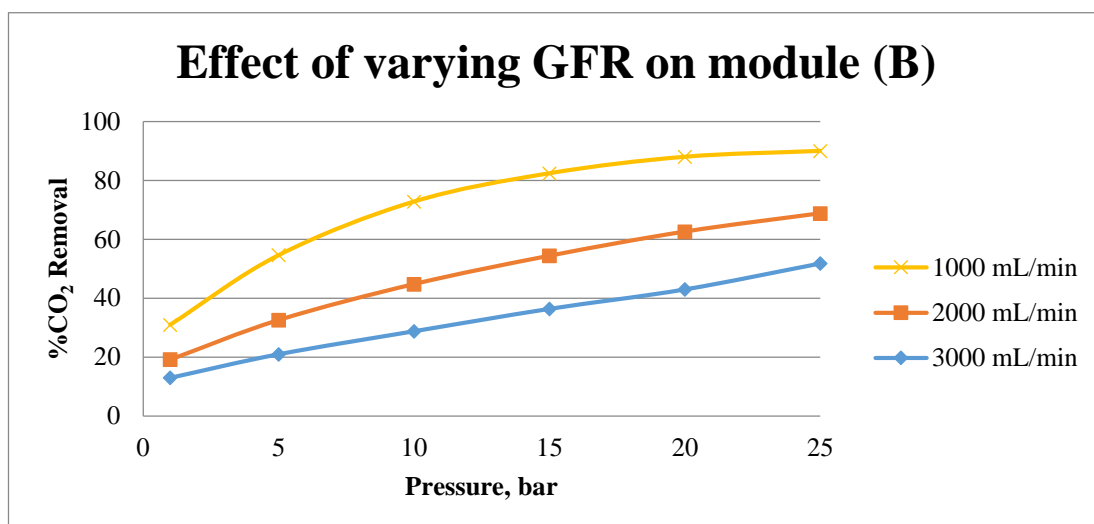


Figure 16: The effect of varying gas flow rate (1000, 2000 and 3000 mL/min) on module (B).

The same trend was obtained for module (B) as seen in Figure 16. Another result observed is that the maximum %CO₂ removal in module (A) was lower than the maximum removal in module (B).

4.2.4 The effect of varying liquid flow rate

Another parameter was studied which is the effect of varying liquid flow rate on modules (A) and (B). For this study, several experiments were conducted. The first experiment objective was to study the effect of varying liquid flow rate for module (A) and the obtained results are presented in Figure 17. The gas flow rate was kept constant at a flow rate of 2000 mL/min while the liquid flow rate was varied among three values (10, 20 and 30 mL/min) using NaOH (1 M) as an absorption solvent.

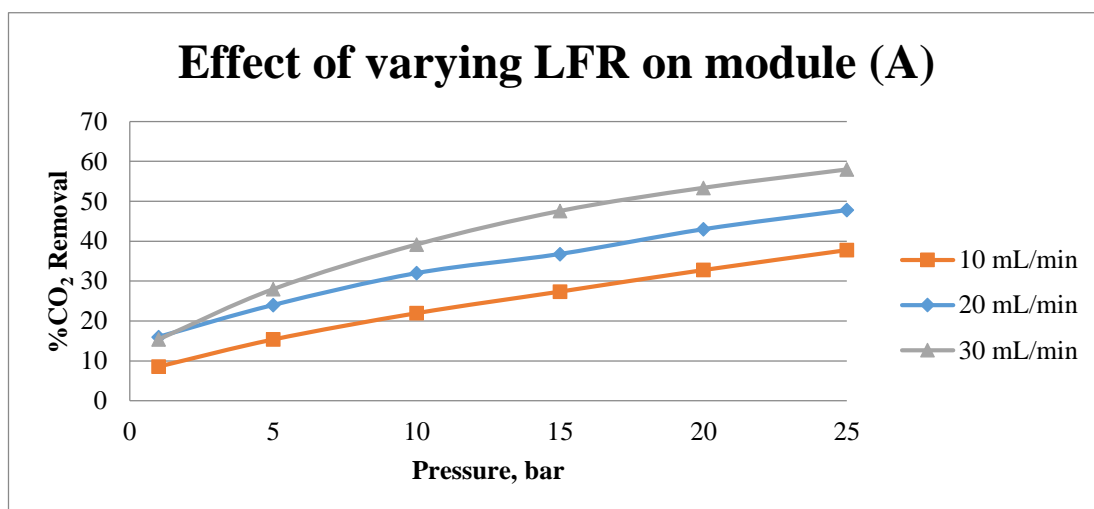


Figure 17: The effect of varying liquid flow rate (10, 20 and 30 mL/min) on module (A) using PFA-HFM at a fixed gas flow rate (2000 mL/min).

The results were in agreement with previous work done by Marzouk (Marzouk et al., 2010) where the %CO₂ removal was expected to be more as the liquid flow rate increases. Increasing the liquid flow rate will reduce the residence time of the solvent which in turn allow more fresh solvent to flow and absorb more.

The same experiment was carried out using module (B) under the same operating conditions and the results were shown in Figure 18.

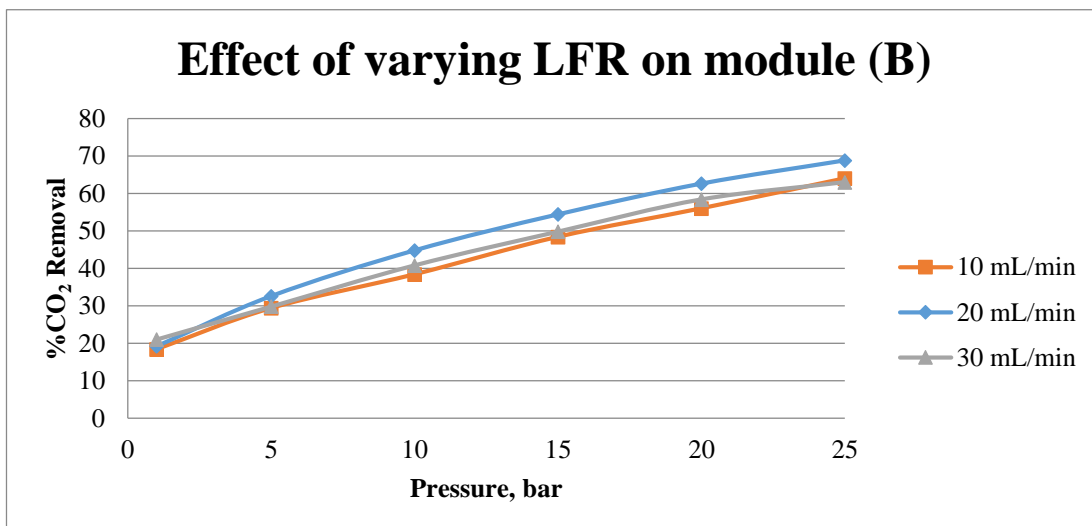


Figure 18: The effect of varying liquid flow rate (10, 20 and 30 mL/min) on module (B) using PFA-HFM at a fixed gas flow rate (2000 mL/min).

As shown in Figure 18, the effect of liquid flow rate had little influence on the %CO₂ removal over the tested pressures. This could be attributed to the enhanced removal efficiency because of the higher liquid velocities compared to the results obtained in module (A) (Figure 17). Again, the maximum %CO₂ removal in module (A) was lower than the maximum removal in module (B).

The same operating conditions were used to study the effect of liquid velocities for both module (A) and (B) and Figure 19 shows the obtained results.

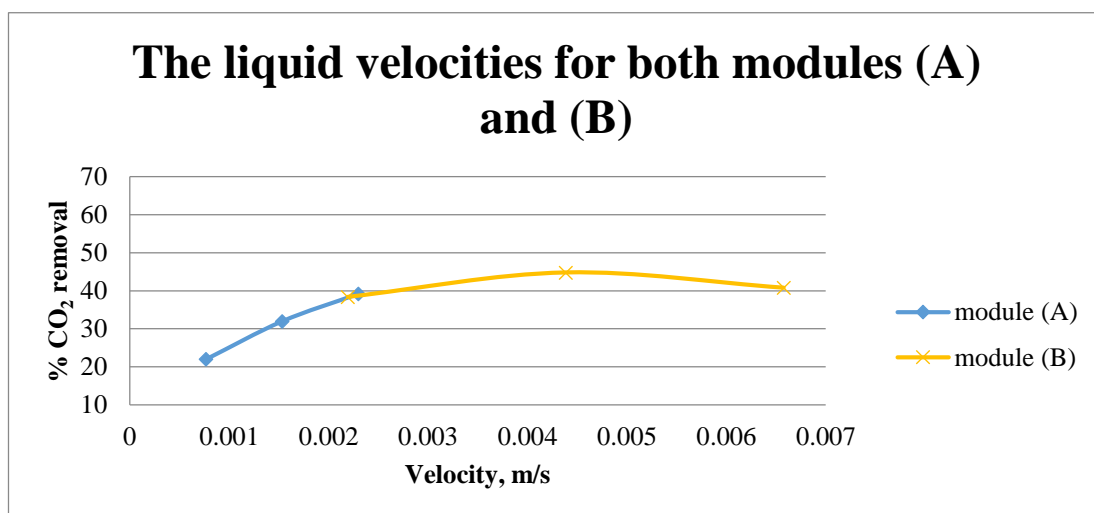


Figure 19: The effect of liquid flow rate on modules (A) & (B) in terms of velocity using PFA-HFM at a fixed gas flow rate (2000 mL/min), aqueous sodium hydroxide flow rates (10, 20 & 30 mL/min) and pressure of 10 bars.

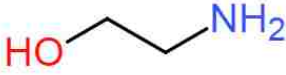
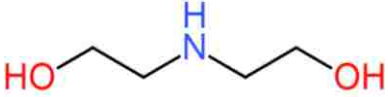
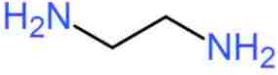
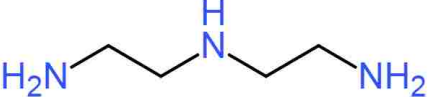
Figure 19 represents the increase in liquid velocities for module (B) compared to module (A). In module (A); increasing the velocity increases %CO₂ removal. Whereas in module (B), the minimum velocity obtained (at a flow rate of 10 mL/min) was almost the same as the maximum velocity in module (A) (at a flow rate of 30 mL/min). For liquid flow rates of 20 and 30 mL/min, no significant changes observed in %CO₂ removal. This could be attributed to solvent saturation (calculations are shown in Appendix C).

4.2.5 Effect of amine type

Depending on the number of hydrogen atoms replaced by functional groups in ammonia molecule, the Amine-based solvent can be classified into; primary amines (MEA), secondary amines (DEA) and tertiary amines (TEA). Another classification depends on the number of nitrogen atoms; tetraethylenepentamine (TEPA) > triethylenetetramine (TETA) > diethylenetriamine (DETA) (Al-Marzouqi, Marzouk, El-Naas, & Abdullatif, 2009).

The name and the chemical structure of amine solvents used are presented in Table 6.

Table 6: Chemical structure of the used amines solvent

Amine	Chemical structure
Monoethanolamine (MEA).	
Diethanolamine (DEA).	
Ethylenediamine (EDA).	
Diethylenetriamine (DETA).	

The effect of Amine types was studied first on module (A) then module (B). For all amines solvents, the solution (1 M) was kept at a flow rate of 20 mL/min while the gas flow rate was kept at 2000 mL/min. Figure 20 presents the effect of different solvent types on %CO₂ removal efficiency using module (A).

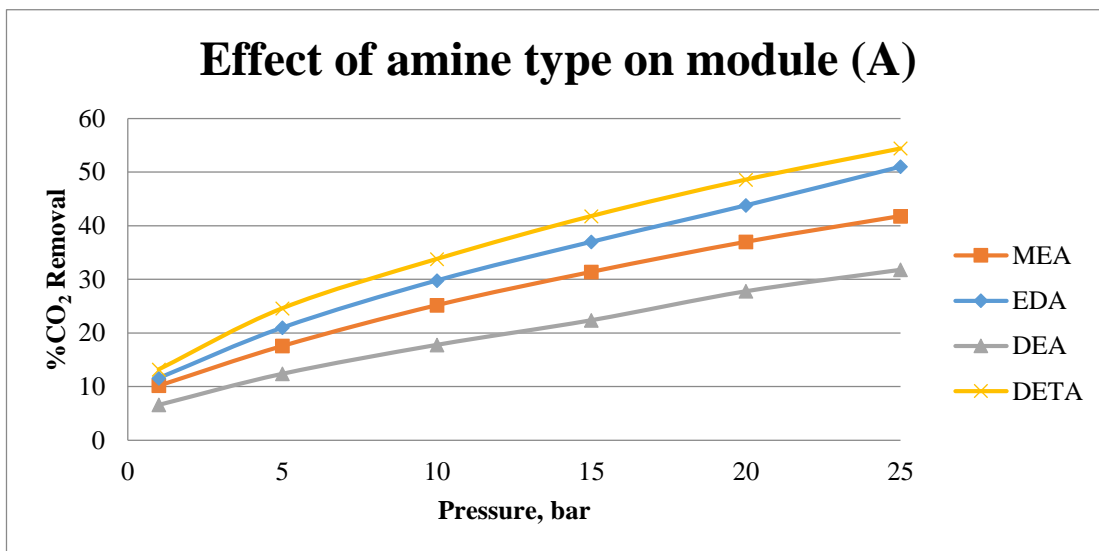


Figure 20: The effect of amine type on module (A) using PFA-HFM at fixed gas flow rate (2000 mL/min) and aqueous sodium hydroxide flow rates (20 mL/min).

When comparing MEA to DEA; increasing number of hydroxyl group causes a reduction in %CO₂ removal which can be explained by the effect of steric hindrance around amine group (Zhao & Winston Ho, 2012). Another comparison was made to investigate the effect of increasing number of amine groups. It was expected to have more %CO₂ removal as we are increasing the number of amine groups. As shown in Figure 20, the highest removal was obtained when using DETA which contained three amine groups then followed by EDA and finally MEA. The reason behind that is the availability of reaction sites increases when increasing number of amine groups as mentioned by (Singh, Niederer, & Versteeg, 2009). Additionally, On the other hand, different results were noticed when using module (B) and Figure 21 shows the obtained results.

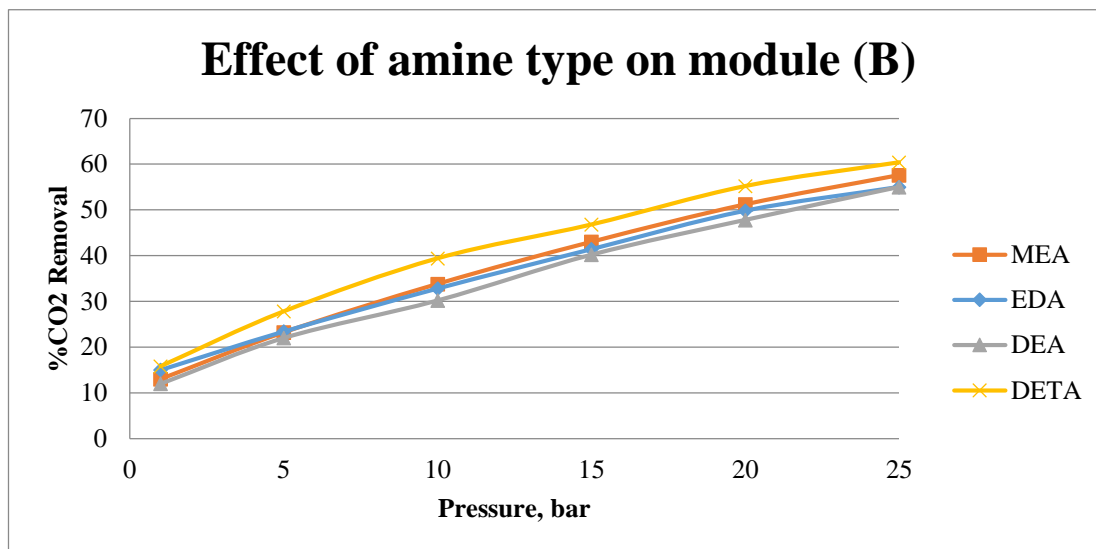


Figure 21: The effect of amine type on module (B) using PFA-HFM at fixed gas flow rate (2000 mL/min) and aqueous sodium hydroxide flow rates (20 mL/min).

The presence of beads eliminated the effect of varying amines solvent on %CO₂ removal efficiency which can be explained by results obtained in section 4.2.4 for module (B).

4.2.6 Inlet solvent concentration

The last parameter studied was the inlet solvent concentration. Three different concentrations were used to explore the effect of solvent concentration on %CO₂ removal efficiency using modules (A) and (B). Both gas and liquid flow rates were kept constant at a rate of 2000 mL/min and 20 mL/min respectively. The solvent used was NaOH of different concentrations (0.25, 0.5 and 1 M). Figure 22 and Figure 23 shows the results obtained for both modules (A) and (B) respectively.

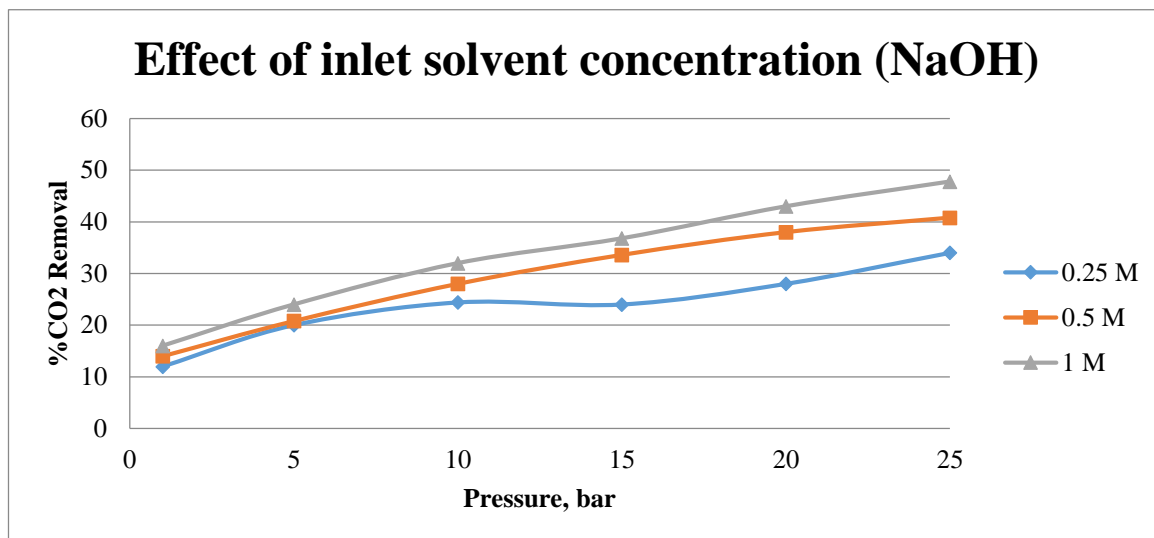


Figure 22: The effect of inlet solvent concentration on module (A) using PFA-HFM at fixed gas flow rate (2000 mL/min) and aqueous sodium hydroxide flow rates (20 mL/min).

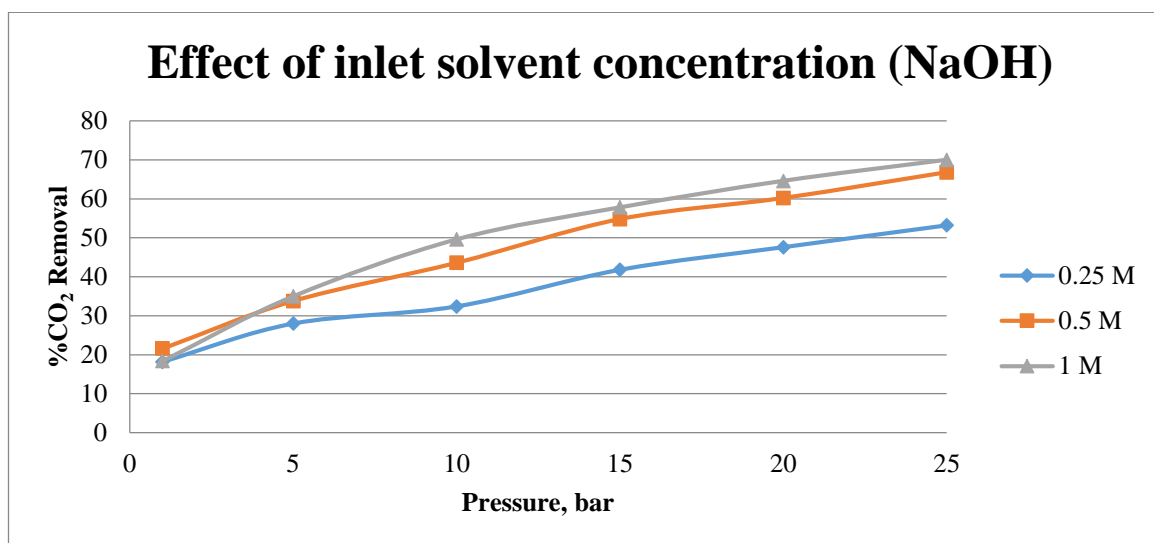


Figure 23: The effect of inlet solvent concentration on module (B) using PFA-HFM at fixed gas flow rate (2000 mL/min) and aqueous sodium hydroxide flow rates (20 mL/min).

As expected and reported by several researchers (Y. S. Kim & Yang, 2000); (R. Wang, Li, & Liang, 2004); (Kumar, Hogendoorn, Feron, & Versteeg, 2002) increasing the inlet solvent concentration increases the %CO₂ removal and this trend

was observed for both modules (A) and (B). The maximum %CO₂ removal was obtained in module (B) compared to module (A).

4.3 Evaluation of the overall mass transfer coefficients for chemical absorption

In this section, overall mass transfer coefficient is evaluated from experimental data and compared with the values calculated from the model which is based on literature correlation.

4.3.1 Theoretical mass transfer coefficient

According to the film theory which illustrates the mass transfer at the interface, the following equation describes the overall mass transfer coefficient for membrane gas absorption based on gas phase (Zydney, 1992):

$$\frac{1}{K_{OG}} = \frac{d_o}{K_G d_i} + \frac{d_o}{K_m d_{lm}} + \frac{1}{mEK_L} \quad \text{Equation 2}$$

Where K_{OG} is the overall mass transfer coefficient (m s^{-1}), K_G , K_M , K_L are the individual mass transfer coefficient of gas, membrane, and liquid (m s^{-1}) respectively. d_{lm} is the logarithmic mean diameters of the membrane fiber (m), m is the solubility of gas in the solvent which accounts for the physical absorption (-), E is the Enhancement factor which counts for chemical reaction (-), and d_i and d_o are the inside and outside diameter of the fiber membrane (m).

The previous equation can be written in terms of resistance in series. This model consists of three major resistances; the gas film resistance, membrane resistance and liquid film resistance:

$$R_{OG} = R_G + R_M + R_L \quad \text{Equation 3}$$

Where R_{OG} is the overall mass transfer resistance ($s\ m^{-1}$), R_G, R_M, R_L are the individual mass transfer resistances of gas film, membrane and liquid film ($s\ m^{-1}$) respectively. Correlations have been used to calculate each parameter. Starting with the individual mass transfer coefficient in the gas phase (K_G), Leveque's correlation (Martin, 2002) is used where the gas flows in the tube side. The correlation is described by Sherwood's number as follow:

$$Sh = \frac{K_G d_i}{D_{CO_2-g}} = 1.62 \left(\frac{d_i}{L} Re Sc \right)^{0.33} \quad \text{Equation 4}$$

Where Re is Reynold's number and Sc is Schmidt number and the two numbers are dimensionless.

The membrane mass transfer coefficient part where it's described by (Kreulen, Smolders, Versteeg, & Van Swaaij, 1993) as follows:

$$K_M = \frac{D_{g,eff} \varepsilon}{\tau \delta} \quad \text{Equation 5}$$

Where $D_{g,eff}$ is the effective diffusion coefficient of gas (CO_2) in the gas mixture ($m^2\ s^{-1}$), ε is the porosity of the membrane (-), τ is tortuosity of membrane (-) and δ is membrane thickness (m).

The effective diffusion coefficient of gas can be calculated by:

$$D_{g,eff} = \left(\frac{1}{D_{g,m}} + \frac{1}{D_{g,Kn}} \right)^{-1} \quad \text{Equation 6}$$

Where $D_{g,m}$ is the molecular diffusion ($m^2\ s^{-1}$) and $D_{g,Kn}$ is Knudsen diffusion ($m^2\ s^{-1}$).

Knudsen number was calculated to evaluate the effect of Knudsen diffusion on the system and the calculations showed a negligible effect for $D_{g,Kn}$. For that reason, the effective diffusion coefficient was replaced with the diffusion coefficient of gas in a mixture (D_{CO_2-g}).

The last correlation used is for the individual mass transfer coefficient in the liquid phase which is defined by Yang and Cussler correlation (Cussler, 2009):

$$Sh = \frac{K_L d_h}{D_{CO_2-L}} = 1.25 \left(\frac{d_h}{L} Re \right)^{0.93} (Sc)^{0.33} \quad \text{Equation 7}$$

Where d_h is the hydraulic diameter (m) and D_{CO_2-L} is the diffusion coefficient of gas (CO_2) in the solvent ($m^2 s^{-1}$).

Two correlations were used to calculate the individual mass transfer coefficient in shell side for module (B); the first correlation is same as the one used for module (A) which is correlation (7) but the only difference here is that the superficial velocity that accounts for beads added to shell side. The other correlation accounts for a fixed bed of beads which is described by:

$$Sh = 1.17 (Re)^{0.58} (Sc)^{0.33} \quad \text{Equation 8}$$

In this correlation, the beads diameter and the superficial velocity are being used.

Table 7 and Table 8 show the physical properties, fiber characteristics, and beads used in calculations.

Table 7: Physical properties used in the calculation

Physical properties	Unit	Value	Reference
Solubility coefficient in the solvent	(-)	0.565	(Faiz & Al-Marzouqi, 2011)
Diffusion coefficient in CH ₄	m^2/s	1.6588E-5	(Cussler, 2009)
Diffusion coefficient in the solvent	m^2/s	1.3806E-9	(Faiz & Al-Marzouqi, 2011)
Density of CO ₂	kg/m^3	1.87	(Marzouk et al., 2012)
Density of CH ₄	kg/m^3	7.0944E-1	(Calculated)
The dynamic viscosity of CH ₄	m^2/s	1.1100E-4	(Makita, Tanaka, & Nagashima, 1973)
The dynamic viscosity of CO ₂	m^2/s	1.3720E-5	(Marzouk et al., 2012)

Table 8: Characteristics of PFA fiber

Fiber characteristics	Unit	Value	Reference
No. of fibers	(-)	300	Measured
Length	m	0.18	Measured
Inside diameter	m	2.5E-4	Measured
Outside diameter	m	6.5E-4	Measured
Thickness	m	2.00E-4	Calculated
Porosity (ϵ)	(-)	0.568	Measured
Tortuosity (τ)	(-)	3.6103	Calculated
Hydraulic diameter	m	1.2980E-3	Calculated
Log mean diameter	m	4.1862E-4	Calculated

The beads used in the system are spherical glass beads and the Table 9 shows its specifications.

Table 9: Beads used in the module

Parameter	Unit	Value
Beads diameter	<i>m</i>	0.001
Specific gravity	(-)	2550
No. of beads	(-)	65

4.3.2 Experimental mass transfer coefficient

For the purpose of evaluating and comparing the results obtained from experimental data to those found theoretically, several equations have been used to calculate the overall mass transfer coefficient based on gas phase and chemical absorption.

The first equation used is (Kreulen, Smolders, Versteeg, & van Swaaij, 1993):

$$K_{OG} = \frac{Q_G}{A} \ln \left(\frac{C_{G,in}}{C_{G,out}} \right) \quad \text{Equation 9}$$

Where Q_G is the volumetric gas flow rate ($\text{m}^3 \text{s}^{-1}$), A is the outer membrane area for all fibers (300 fiber) (m^2), $C_{G,in}$ and $C_{G,out}$ are the inlet and outlet gas concentration (mol L^{-1}) respectively.

4.3.3 Individual MTC for module A & B based on theory.

Figure 24 represents the individual MTCs for gas and membrane side in both modules (A) and (B) whereas Figure 25 shows the individual MTC for module (A) and (B).

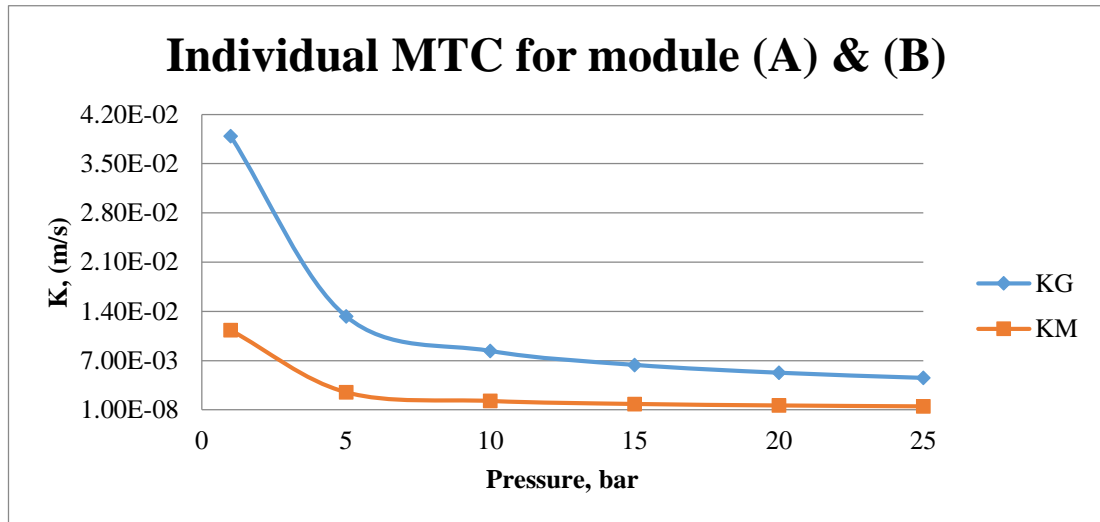


Figure 24: Individual MTC for module (A) & (B) for gas film and membrane using PFA-HFM at fixed gas flow rate (2000 mL/min) and aqueous sodium hydroxide flow rates (20 mL/min).

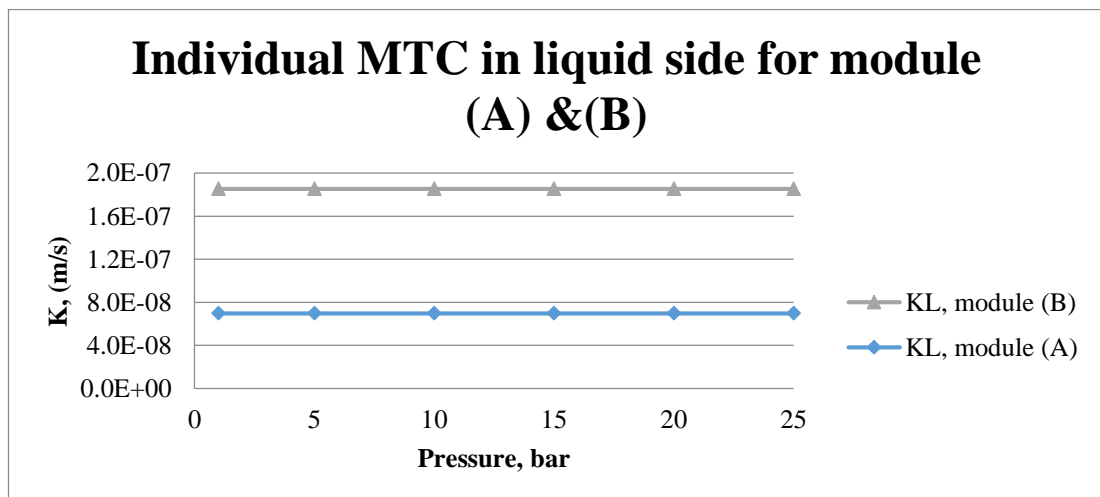


Figure 25: Individual MTC for module (A) & (B) for liquid film using PFA-HFM at fixed gas flow rate (2000 mL/min) and aqueous sodium hydroxide flow rates (20 mL/min).

Figure 24 shows the individual mass transfer coefficient for gas film and membrane (K_G and K_M) are decreasing as the pressure increase while in Figure 25, the individual mass transfer in the liquid film (K_L) is almost constant along the pressure trend. This can be explained by referring to correlations (4, 5 & 7) used for each individual MTC. Starting with mass transfer coefficient in the gas phase (K_G); it's

inversely proportional to diffusion coefficient ($D_{\text{CO}_2\text{-g}}$) by a factor of 1/3 and at the same time the diffusion coefficient is inversely proportional to pressure. Then, as the pressure is increasing the diffusion coefficient will decrease and K_G will increase. The gas phase resistance is the reciprocal of K_G which means increasing K_G will cause a reduction in resistance with increasing pressure. The same explanation applies for membrane resistance but the individual mass transfer coefficient in the gas phase (K_M) is proportional to diffusion coefficient ($D_{\text{CO}_2\text{-g}}$).

For the liquid film, the individual mass transfer coefficient (K_L) is calculated for an incompressible fluid where the effect of pressure is negligible. Based on the correlation used for mass transfer coefficient calculations, all terms are considered to be constant which can explain the constant value of K_L with increasing the pressure.

In module (B), a known number of spherical glass beads (65 g) were added to the module to increase the velocity of the fluid. This increasing of the fluid velocity will increase the individual mass transfer of the liquid (K_L).

4.3.4 Overall MTC for module A & B theoretically and experimentally

The three individual MTCs were combined to find the overall MTC (K_{OG}) and the theoretical values were compared with experimental results.

Figure 26 and Figure 27 represent the theoretical and the experimental overall MTC for each module; A and B.

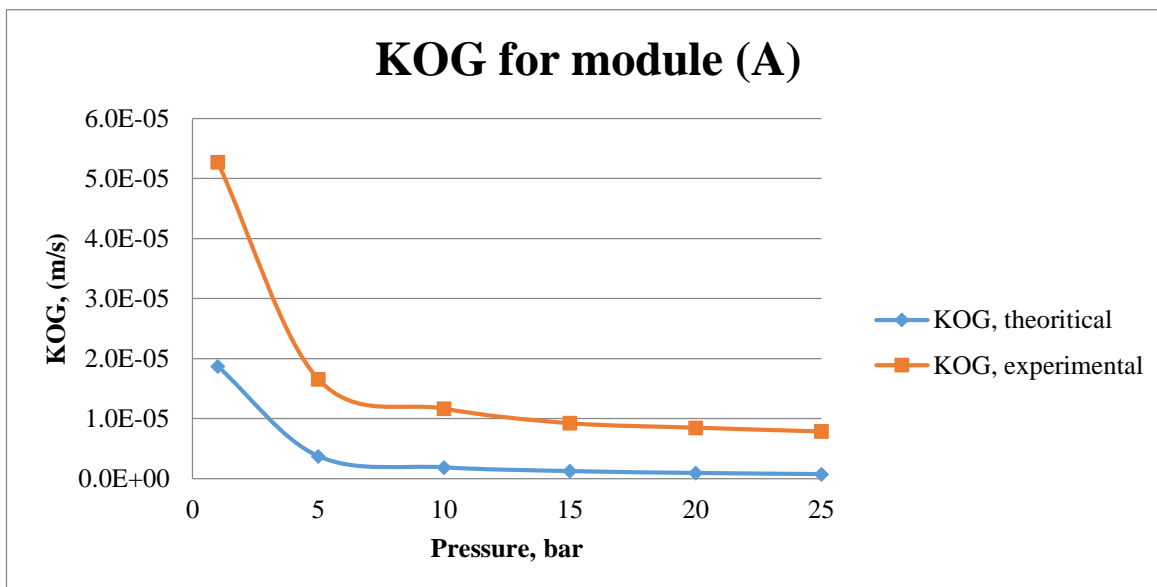


Figure 26: Comparison between overall mass transfer coefficients based on theoretical and experimental correlations for module (A) using PFA-HFM at fixed gas flow rate (2000 mL/min) and aqueous sodium hydroxide flow rates (20 mL/min).

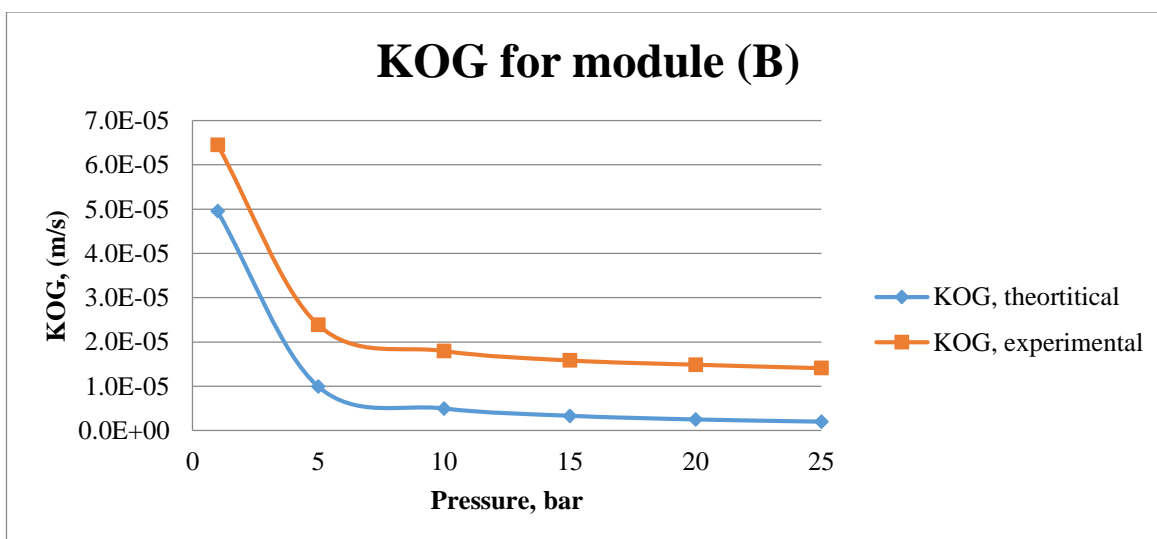


Figure 27: Comparison between overall mass transfer coefficients based on theoretical and experimental correlations for module (B) using PFA-HFM at fixed gas flow rate (2000 mL/min) and aqueous sodium hydroxide flow rates (20 mL/min).

As seen from Figure 26 and Figure 27, there is a good agreement between the theory MTC and those obtained from the experimental values. The difference can be explained by the fact that the equations used for theoretical calculation of MTC were

solely based on the chemical and physical properties found from literature and the geometry of the membrane contactor. On the other hand, the experimental equation was based on the experimental data.

The theoretical overall MTC for both modules (A) and (B) are shown in Figure 28

whereas Figure 29 shows the experimental overall MTC for modules (A) and (B).

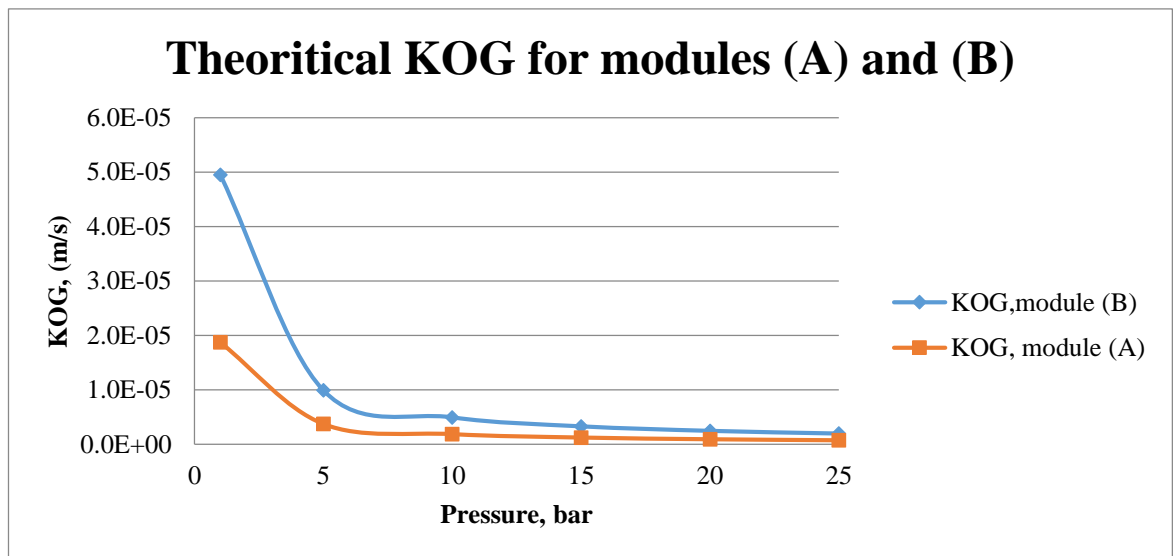


Figure 28: Theoretical overall MTC using PFA-HFM at fixed gas flow rate (2000 mL/min) and aqueous sodium hydroxide flow rates (20 mL/min) for module (A) and (B).

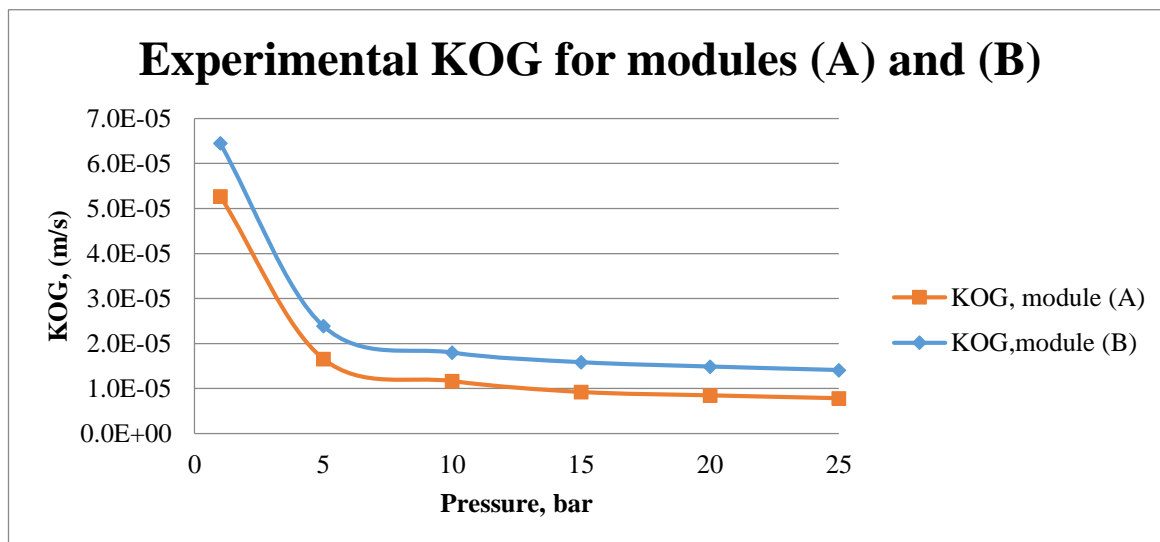


Figure 29: Experimental overall MTC using PFA-HFM at fixed gas flow rate (2000 mL/min) and aqueous sodium hydroxide flow rates (20 mL/min) for module (A) and (B).

As seen from Figure 28 and Figure 29, module (B) showed higher values compared to module (A) for both theoretical and experimental overall MTC which is in agreement with previous discussion.

In order to weigh the validity of using the same correlation (8), a comparison between correlations (7) and (8) was made and Figure30 shows the results obtained.

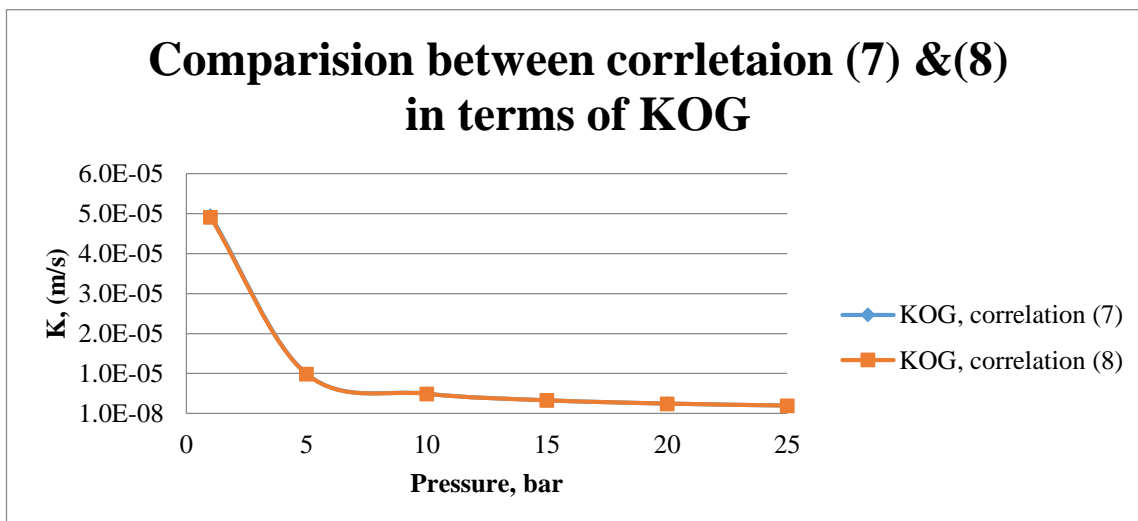


Figure 30: Overall MTC using correlation (7) & (8) using PFA-HFM at fixed gas flow rate (2000 mL/min) and aqueous sodium hydroxide flow rates (20 mL/min).

Figure 30 concludes the validity of using correlation (7) or (8) to represent the MTC for the packed module (B).

Chapter 5: Conclusions

Undoubtedly, the alternative technique which is the gas absorption membrane showed an improvement in removal efficiency and reducing the operational and economic issues governed by conventional separation processes. The custom-made hollow fiber membrane contactors packed with glass beads showed up to 20% improvement in %CO₂ removal compared to those of non-packed modules. Operational parameters were studied and concluded their significant effect on %CO₂ removal efficiency. Increasing the beads size reduced the %CO₂ removal due to increase in fluid velocity. Additionally, decreasing the gas flow rate and increasing the inlet solvent concentration increased %CO₂ removal.

For the packed module, a potential result found from an experiment in terms of varying liquid flow rate; increasing the liquid flow rate had an insignificant effect on removal efficiency. The same result was obtained when varying the solvent type. Theoretical overall mass transfer coefficient model was compared to experimental overall MTC for both modules (A) & (B) and the results showed good agreement between the experimental and theoretical one's values. The development of custom-made hollow fiber membrane contactors could be further studied and evaluated in terms of stripping.

References

- Al-Marzouqi, M. H., El-Naas, M. H., Marzouk, S. A. M., Al-Zarooni, M. A., Abdullatif, N., & Faiz, R. (2008). Modeling of CO₂ absorption in membrane contactors. *Separation and Purification Technology*, 59(3), 286-293. doi:<http://dx.doi.org/10.1016/j.seppur.2007.06.020>
- Al-Marzouqi, M. H., Marzouk, S. A. M., & Abdullatif, N. (2017). High pressure removal of acid gases using hollow fiber membrane contactors: Further characterization and long-term operational stability. *Journal of Natural Gas Science and Engineering*, 37, 192-198. doi:<https://doi.org/10.1016/j.jngse.2016.11.039>
- Al-Marzouqi, M. H., Marzouk, S. A. M., El-Naas, M. H., & Abdullatif, N. (2009). CO₂ Removal from CO₂-CH₄ Gas Mixture Using Different Solvents and Hollow Fiber Membranes. *Industrial & Engineering Chemistry Research*, 48(7), 3600-3605. doi:10.1021/ie800977z
- Al-saffar, H. B., Ozturk, B., & Hughes, R. (1997). A Comparison of Porous and Non-Porous Gas-Liquid Membrane Contactors for Gas Separation. *Chemical Engineering Research and Design*, 75(7), 685-692. doi:<https://doi.org/10.1205/026387697524182>
- Atcharyawut, S., Feng, C., Wang, R., Jiratananon, R., & Liang, D. T. (2006). Effect of membrane structure on mass-transfer in the membrane gas-liquid contacting process using microporous PVDF hollow fibers. *Journal of Membrane Science*, 285(1), 272-281. doi:<https://doi.org/10.1016/j.memsci.2006.08.029>
- Atcharyawut, S., Jiratananon, R., & Wang, R. (2007). Separation of CO₂ from CH₄ by using gas-liquid membrane contacting process. *Journal of Membrane Science*, 304(1), 163-172. doi:<https://doi.org/10.1016/j.memsci.2007.07.030>
- Bothun, G. D., Knutson, B. L., Strobel, H. J., Nokes, S. E., Brignole, E. A., & Díaz, S. (2003). Compressed solvents for the extraction of fermentation products within a hollow fiber membrane contactor. *The Journal of Supercritical Fluids*, 25(2), 119-134. doi:[https://doi.org/10.1016/S0896-8446\(02\)00093-1](https://doi.org/10.1016/S0896-8446(02)00093-1)
- Brunetti, A., Scura, F., Barbieri, G., & Drioli, E. (2010). Membrane technologies for CO₂ separation. *Journal of Membrane Science*, 359(1), 115-125. doi:<https://doi.org/10.1016/j.memsci.2009.11.040>
- Cambridge University press, C., UK. (2005). Intergovernmental Panel on Climate Change (IPCC) Special Report on Carbon Dioxide Capture and Storage.
- Choi, S. U. S., & Eastman, J. (1995). *Enhancing thermal conductivity of fluids with nanoparticles* (Vol. 66).

- Cui, Z., & deMontigny, D. (2017). Experimental study of carbon dioxide absorption into aqueous ammonia with a hollow fiber membrane contactor. *Journal of Membrane Science*, 540, 297-306.
doi:<https://doi.org/10.1016/j.memsci.2017.06.013>
- Cussler, E. L. (2009). *Diffusion: mass transfer in fluid systems*: Cambridge university press.
- Darabi, M., Rahimi, M., & Molaei Dehkordi, A. (2017). Gas absorption enhancement in hollow fiber membrane contactors using nanofluids: Modeling and simulation. *Chemical Engineering and Processing: Process Intensification*, 119, 7-15. doi:<https://doi.org/10.1016/j.cep.2017.05.007>
- Davison, J. (2007). Performance and costs of power plants with capture and storage of CO₂. *Energy*, 32(7), 1163-1176.
doi:<https://doi.org/10.1016/j.energy.2006.07.039>
- deMontigny, D., Tontiwachwuthikul, P., & Chakma, A. (2006). Using polypropylene and polytetrafluoroethylene membranes in a membrane contactor for CO₂ absorption. *Journal of Membrane Science*, 277(1), 99-107.
doi:<https://doi.org/10.1016/j.memsci.2005.10.024>
- Dickson, J. M., Childs, R. F., McCarry, B. E., & Gagnon, D. R. (1998). Development of a coating technique for the internal structure of polypropylene microfiltration membranes. *Journal of Membrane Science*, 148(1), 25-36.
doi:[https://doi.org/10.1016/S0376-7388\(98\)00142-2](https://doi.org/10.1016/S0376-7388(98)00142-2)
- Dindore, V. Y., Brillman, D. W. F., Feron, P. H. M., & Versteeg, G. F. (2004). CO₂ absorption at elevated pressures using a hollow fiber membrane contactor. *Journal of Membrane Science*, 235(1), 99-109.
doi:<https://doi.org/10.1016/j.memsci.2003.12.029>
- Faiz, R., & Al-Marzouqi, M. (2010). CO₂ removal from natural gas at high pressure using membrane contactors: Model validation and membrane parametric studies. *Journal of Membrane Science*, 365(1-2), 232-241.
doi:<http://dx.doi.org/10.1016/j.memsci.2010.09.004>
- Faiz, R., & Al-Marzouqi, M. (2011). Insights on natural gas purification: Simultaneous absorption of CO₂ and H₂S using membrane contactors. *Separation and Purification Technology*, 76(3), 351-361.
doi:<https://doi.org/10.1016/j.seppur.2010.11.005>
- Feng, C., Wang, R., Zhang, H., & Shi, L. (2011). Diverse morphologies of PVDF hollow fiber membranes and their performance analysis as gas/liquid contactors. *Journal of Applied Polymer Science*, 119(3), 1259-1267.
doi:[10.1002/app.30250](https://doi.org/10.1002/app.30250)

- Gabriel, E. M., & Gillberg, G. E. (1993). In situ modification of microporous membranes. *Journal of Applied Polymer Science*, 48(12), 2081-2090. doi:10.1002/app.1993.070481202
- Golkhar, A., Keshavarz, P., & Mowla, D. (2013). Investigation of CO₂ removal by silica and CNT nanofluids in microporous hollow fiber membrane contactors. *Journal of Membrane Science*, 433, 17-24. doi:http://dx.doi.org/10.1016/j.memsci.2013.01.022
- Hedayat, M., Soltanieh, M., & Mousavi, S. A. (2011). Simultaneous separation of H₂S and CO₂ from natural gas by hollow fiber membrane contactor using mixture of alkanolamines. *Journal of Membrane Science*, 377(1-2), 191-197. doi:10.1016/j.memsci.2011.04.051
- Jin, P., Huang, C., Shen, Y., Zhan, X., Hu, X., Wang, L., & Wang, L. (2017). Simultaneous Separation of H₂S and CO₂ from Biogas by Gas-Liquid Membrane Contactor Using Single and Mixed Absorbents. *Energy & Fuels*, 31(10), 11117-11126. doi:10.1021/acs.energyfuels.7b02114
- Kang, G., Chan, Z. P., Saleh, S. B. M., & Cao, Y. (2017). Removal of high concentration CO₂ from natural gas using high pressure membrane contactors. *International Journal of Greenhouse Gas Control*, 60, 1-9. doi:https://doi.org/10.1016/j.ijggc.2017.03.003
- Khaisri, S., deMontigny, D., Tontiwachwuthikul, P., & Jiraratananon, R. (2009). Comparing membrane resistance and absorption performance of three different membranes in a gas absorption membrane contactor. *Separation and Purification Technology*, 65(3), 290-297. doi:http://dx.doi.org/10.1016/j.seppur.2008.10.035
- Kim, B.-S., & Harriott, P. (1987). Critical entry pressure for liquids in hydrophobic membranes. *Journal of Colloid and Interface Science*, 115(1), 1-8. doi:https://doi.org/10.1016/0021-9797(87)90002-6
- Kim, Y., & Lee, S. (2000). Stable nonconforming quadrilateral finite elements for the Stokes problem. *Applied Mathematics and Computation*, 115(2), 101-112. doi:https://doi.org/10.1016/S0096-3003(99)00145-9
- Kim, Y. S., & Yang, S. M. (2000). Absorption of carbon dioxide through hollow fiber membranes using various aqueous absorbents. *Separation and Purification Technology*, 21(1-2), 101-109. doi:10.1016/S1383-5866(00)00195-7
- Kreulen, H., Smolders, C. A., Versteeg, G. F., & Van Swaaij, W. P. M. (1993). Determination of mass transfer rates in wetted and non-wetted microporous membranes. *Chemical Engineering Science*, 48(11), 2093-2102. doi:https://doi.org/10.1016/0009-2509(93)80084-4

- Kreulen, H., Smolders, C. A., Versteeg, G. F., & van Swaaij, W. P. M. (1993). Microporous hollow fibre membrane modules as gas-liquid contactors Part 2. Mass transfer with chemical reaction. *Journal of Membrane Science*, 78(3), 217-238. doi:[https://doi.org/10.1016/0376-7388\(93\)80002-F](https://doi.org/10.1016/0376-7388(93)80002-F)
- Kumar, P. S., Hogendoorn, J. A., Feron, P. H. M., & Versteeg, G. F. (2002). New absorption liquids for the removal of CO₂ from dilute gas streams using membrane contactors. *Chemical Engineering Science*, 57(9), 1639-1651. doi:10.1016/S0009-2509(02)00041-6
- Leung, D. Y. C., Caramanna, G., & Maroto-Valer, M. M. (2014). An overview of current status of carbon dioxide capture and storage technologies. *Renewable and Sustainable Energy Reviews*, 39, 426-443. doi:<https://doi.org/10.1016/j.rser.2014.07.093>
- Li, J.-L., & Chen, B.-H. (2005). Review of CO₂ absorption using chemical solvents in hollow fiber membrane contactors. *Separation and Purification Technology*, 41(2), 109-122. doi:<https://doi.org/10.1016/j.seppur.2004.09.008>
- Li, K., & Teo, W. K. (1998). Use of permeation and absorption methods for CO₂ removal in hollow fibre membrane modules. *Separation and Purification Technology*, 13(1), 79-88. doi:[https://doi.org/10.1016/S1383-5866\(97\)00059-2](https://doi.org/10.1016/S1383-5866(97)00059-2)
- Mackie, J., & Meares, P. (1955). *The diffusion of electrolytes in a cation-exchange resin membrane I. Theoretical*. Paper presented at the Proc. R. Soc. Lond. A.
- Makita, T., Tanaka, Y., & Nagashima, A. (1973). Evaluation and correlation of viscosity data: the most probable values of the viscosity of gaseous methane. *The Review of Physical Chemistry of Japan*, Vol.43 No.1, 1-6.
- Mansourizadeh, A., & Ismail, A. F. (2009). Hollow fiber gas-liquid membrane contactors for acid gas capture: A review. *Journal of Hazardous Materials*, 171(1-3), 38-53. doi:<http://dx.doi.org/10.1016/j.jhazmat.2009.06.026>
- Martin, H. (2002). *THE GENERALIZED LÉVÊQUE EQUATION AND ITS USE TO PREDICT HEAT OR MASS TRANSFER FROM FLUID FRICTION* Paper presented at the 20th National Heat Transfer Conference, Italy.
- Marzouk, S. A. M., Al-Marzouqi, M. H., El-Naas, M. H., Abdullatif, N., & Ismail, Z. M. (2010). Removal of carbon dioxide from pressurized CO₂-CH₄ gas mixture using hollow fiber membrane contactors. *Journal of Membrane Science*, 351(1-2), 21-27. doi:<http://dx.doi.org/10.1016/j.memsci.2010.01.023>

- Marzouk, S. A. M., Al-Marzouqi, M. H., Teramoto, M., Abdullatif, N., & Ismail, Z. M. (2012). Simultaneous removal of CO₂ and H₂S from pressurized CO₂–H₂S–CH₄ gas mixture using hollow fiber membrane contactors. *Separation and Purification Technology*, 86, 88-97. doi:<https://doi.org/10.1016/j.seppur.2011.10.024>
- Mavroudi, M., Kaldis, S. P., & Sakellaropoulos, G. P. (2003). Reduction of CO₂ emissions by a membrane contacting process☆. *Fuel*, 82(15–17), 2153-2159. doi:[http://dx.doi.org/10.1016/S0016-2361\(03\)00154-6](http://dx.doi.org/10.1016/S0016-2361(03)00154-6)
- Mika, A. M., Childs, R. F., Dickson, J. M., McCarry, B. E., & Gagnon, D. R. (1995). A new class of polyelectrolyte-filled microfiltration membranes with environmentally controlled porosity. *Journal of Membrane Science*, 108(1), 37-56. doi:[https://doi.org/10.1016/0376-7388\(95\)00140-2](https://doi.org/10.1016/0376-7388(95)00140-2)
- Mohammaddoost, H., Azari, A., Ansarpour, M., & Osfouri, S. (2018). Experimental investigation of CO₂ removal from N₂ by metal oxide nanofluids in a hollow fiber membrane contactor. *International Journal of Greenhouse Gas Control*, 69, 60-71. doi:<https://doi.org/10.1016/j.ijggc.2017.12.012>
- Nishikawa, N., Ishibashi, M., Ohta, H., Akutsu, N., Matsumoto, H., Kamata, T., & Kitamura, H. (1995). CO₂ removal by hollow-fiber gas-liquid contactor. *Energy Conversion and Management*, 36(6), 415-418. doi:[https://doi.org/10.1016/0196-8904\(95\)00033-A](https://doi.org/10.1016/0196-8904(95)00033-A)
- Nymeijer, D. C., Folkers, B., Breebaart, I., Mulder, M. H. V., & Wessling, M. (2004). Selection of top layer materials for gas–liquid membrane contactors. *Journal of Applied Polymer Science*, 92(1), 323-334. doi:10.1002/app.20006
- Peyravi, A., Keshavarz, P., & Mowla, D. (2015). Experimental Investigation on the Absorption Enhancement of CO₂ by Various Nanofluids in Hollow Fiber Membrane Contactors. *Energy & Fuels*, 29(12), 8135-8142. doi:10.1021/acs.energyfuels.5b01956
- Qi, Z., & Cussler, E. L. (1985). Microporous hollow fibers for gas absorption. *Journal of Membrane Science*, 23(3), 321-332. doi:[http://dx.doi.org/10.1016/S0376-7388\(00\)83149-X](http://dx.doi.org/10.1016/S0376-7388(00)83149-X)
- R.B. Bird, W. E. S., E.N. Lightfoot. (1960). *Transport Phenomena*. New York: John Wiley and Sons.
- Rajabzadeh, S., Yoshimoto, S., Teramoto, M., Al-Marzouqi, M., & Matsuyama, H. (2009). CO₂ absorption by using PVDF hollow fiber membrane contactors with various membrane structures. *Separation and Purification Technology*, 69(2), 210-220. doi:<https://doi.org/10.1016/j.seppur.2009.07.021>

- Ren, J., Wang, R., Zhang, H.-Y., Li, Z., Liang, D. T., & Tay, J. H. (2006). Effect of PVDF dope rheology on the structure of hollow fiber membranes used for CO₂ capture. *Journal of Membrane Science*, 281(1), 334-344. doi:<https://doi.org/10.1016/j.memsci.2006.04.003>
- Rezaei, M., Ismail, A. F., Hashemifard, S. A., & Matsuura, T. (2014). Preparation and characterization of PVDF-montmorillonite mixed matrix hollow fiber membrane for gas-liquid contacting process. *Chemical Engineering Research and Design*, 92(11), 2449-2460. doi:<http://dx.doi.org/10.1016/j.cherd.2014.02.019>
- Singh, P., Niederer, J. P. M., & Versteeg, G. F. (2009). Structure and activity relationships for amine-based CO₂ absorbents-II. *Chemical Engineering Research and Design*, 87(2), 135-144. doi:<https://doi.org/10.1016/j.cherd.2008.07.014>
- Songolzadeh, M., Soleimani, M., Takht Ravanchi, M., & Songolzadeh, R. (2014). Carbon Dioxide Separation from Flue Gases: A Technological Review Emphasizing Reduction in Greenhouse Gas Emissions. *The Scientific World Journal*, 2014, 1-34. doi:10.1155/2014/828131
- Turchetti, M. C. A. L. M. V. P. L. (2017). *Artificial Organ Engineering*. In (pp. XV, 265). doi:<https://doi.org/10.1007/978-1-4471-6443-2>
- Verma, S., & Tiwari, A. (2017). Characterization of Nanofluids as an advanced heat transporting medium for Energy Systems. *Materials Today: Proceedings*, 4(2), 4095-4103.
- Wang, D., Li, K., & Teo, W. K. (2000). Porous PVDF asymmetric hollow fiber membranes prepared with the use of small molecular additives. *Journal of Membrane Science*, 178(1), 13-23. doi:[https://doi.org/10.1016/S0376-7388\(00\)00460-9](https://doi.org/10.1016/S0376-7388(00)00460-9)
- Wang, D., Teo, W. K., & Li, K. (2002). Removal of H₂S to ultra-low concentrations using an asymmetric hollow fibre membrane module. *Separation and Purification Technology*, 27(1), 33-40. doi:[https://doi.org/10.1016/S1383-5866\(01\)00186-1](https://doi.org/10.1016/S1383-5866(01)00186-1)
- Wang, K. L., & Cussler, E. L. (1993). Baffled membrane modules made with hollow fiber fabric. *Journal of Membrane Science*, 85(3), 265-278. doi:[https://doi.org/10.1016/0376-7388\(93\)85280-A](https://doi.org/10.1016/0376-7388(93)85280-A)
- Wang, M., Lawal, A., Stephenson, P., Sidders, J., & Ramshaw, C. (2011). Post-combustion CO₂ capture with chemical absorption: A state-of-the-art review. *Chemical Engineering Research and Design*, 89(9), 1609-1624. doi:<https://doi.org/10.1016/j.cherd.2010.11.005>

- Wang, R., Li, D. F., & Liang, D. T. (2004). Modeling of CO₂ capture by three typical amine solutions in hollow fiber membrane contactors. *Chemical Engineering and Processing: Process Intensification*, 43(7), 849-856. doi:10.1016/S0255-2701(03)00105-3
- Xu, Z., Wang, J., Shen, L., Men, D., & Xu, Y. (2002). Microporous polypropylene hollow fiber membrane: Part I. Surface modification by the graft polymerization of acrylic acid. *Journal of Membrane Science*, 196(2), 221-229. doi:https://doi.org/10.1016/S0376-7388(01)00600-7
- Yang, M.-C., & Cussler, E. L. (1986). Designing hollow-fiber contactors. *AIChE Journal*, 32(11), 1910-1916. doi:10.1002/aic.690321117
- Yoo, M., Han, S.-J., & Wee, J.-H. (2013). Carbon dioxide capture capacity of sodium hydroxide aqueous solution. *Journal of Environmental Management*, 114, 512-519. doi:https://doi.org/10.1016/j.jenvman.2012.10.061
- Zanfir, M., Gavriilidis, A., Wille, C., & Hessel, V. (2005). Carbon Dioxide Absorption in a Falling Film Microstructured Reactor: Experiments and Modeling. *Industrial & Engineering Chemistry Research*, 44(6), 1742-1751. doi:10.1021/ie049726k
- Zha, F. F., Fane, A. G., Fell, C. J. D., & Schofield, R. W. (1992). Critical displacement pressure of a supported liquid membrane. *Journal of Membrane Science*, 75(1), 69-80. doi:https://doi.org/10.1016/0376-7388(92)80007-7
- Zhang Z.E., Y. Y. F., Zhang L. and Ju S.X. (2014). Hollow fiber membrane contactor absorption of CO₂ from the flue gas: Review and perspective. *Global NEST Journal*, 16(2), 354-373.
- Zhao, Y., & Winston Ho, W. S. (2012). Steric hindrance effect on amine demonstrated in solid polymer membranes for CO₂ transport. *Journal of Membrane Science*, 415-416, 132-138. doi:https://doi.org/10.1016/j.memsci.2012.04.044
- Zydney, A. L. (1992). *Membrane handbook* In a. K. K. S. W. S. Winston Ho, Van Nostrand Reinhold (Ed.), (pp. 954 pp). doi:https://doi.org/10.1002/aic.690411024

Appendices

Appendix A: Calculations of %CO₂ Removal and CO₂ Flux

The CO₂ flux was calculating using Equation 10:

$$CO_2 \text{ Flux} \left(\frac{\text{mol}}{\text{m}^2 \cdot \text{min}} \right) = \frac{GFR (CO_{2,in} - CO_{2,out})}{A_{out}} \quad \text{Equation 10}$$

The inlet and the outlet concentrations of CO₂ in the gas mixture were calculated based on:

$$CO_{2,in} \left(\frac{\text{mol}}{\text{L}} \right) = \frac{\%CO_{2,in} * P_{@1atm}}{100 * R T}$$

$$CO_{2,out} \left(\frac{\text{mol}}{\text{L}} \right) = \frac{\%CO_{2,out} * P_{@1atm}}{100 * R T}$$

The area of the tube based on the outer diameter (A_{out}) is defined by:

$$A_{out}(\text{m}^2) = \pi d_{out} L \text{ No. of Fibers}$$

The %CO₂ removal was calculated by Equation 11 :

$$CO_2 \text{ Removal}(\%) = \frac{(CO_{2,in} - CO_{2,out})}{CO_{2,in}} * 100 \quad \text{Equation 11}$$

Table 10 shows the parameters used in the above equations.

Table 10: Parameters used in %CO₂ removal and CO₂ flux calculations

Parameter	Unit	Value
$CO_{2,in}$	%	5
$CO_{2,out}$	%	Measured
Gas constant (R)	$L atm / K mol$	0.082057
Temperature (T)	K	295
Gas flow rate (GFR)	mL / min	2000
Length (L)	m	0.18
No. of fibers	(-)	300
Fiber outer diameter (d_{out})	m	0.65E-3

Sample calculations:

For module without beads where the gas flowing at a flow rate of 2000 mL/min and aqueous sodium hydroxide flowing at a flow rate of 20 mL/min, the CO₂ flux and the %CO₂ removal were calculated as follow:

$$A_{out} = 2\pi (3.25E - 4 m)(0.18m)(300) = 0.11 m^2$$

$$\text{Inlet concentration: } CO_{2,in} \left(\frac{mol}{L} \right) = \frac{\%5 * 1 atm}{100 * (0.082057 \frac{L atm}{K mol})(295 K)} = 2.07E - 3$$

$$\text{Outlet concentration: } CO_{2,out} \left(\frac{mol}{L} \right) = \frac{\%4.2 * 1 atm}{100 * (0.082057 \frac{L atm}{K mol})(295 K)} = 1.73E - 3$$

$$\text{The } CO_2 \text{ flux: } CO_2 \text{ Flux} \left(\frac{mol}{m^2 \cdot min} \right) = \frac{(2000 \frac{mL}{min})(2.07E-3 - 1.73E-3) \left(\frac{mol}{L} \right)}{1000 * 0.11 m^2} = 5.51E - 3$$

$$\text{The \%CO}_2 \text{ removal: } \%CO_2 \text{ Removal}(\%) = \frac{(2.07E-3 - 1.73E-3) \left(\frac{mol}{L} \right)}{2.07E-3 \left(\frac{mol}{L} \right)} * 100 = 16$$

Appendix B: Calculations of theoretical Mass Transfer Coefficient

B.1 The overall mass transfer coefficient

The theoretical overall mass transfer coefficient was calculated based on gas phase:

$$\frac{1}{K_{OG}} = \frac{d_o}{K_G d_i} + \frac{d_o}{K_m d_{lm}} + \frac{1}{mEK_L} \quad \text{Equation 12}$$

Where K_{OG} is the overall mass transfer coefficient (m s^{-1}), K_G , K_M , K_L are the individual mass transfer coefficient of gas film, membrane and liquid film (m s^{-1}) respectively. d_{lm} is the logarithmic mean diameter of the membrane fiber (m), m is solubility of CO_2 which counts for physical absorption (-), E is the Enhancement factor which counts for chemical reaction (-), and d_i and d_o are the inside and outside diameter of the fiber membrane (m).

- Solubility of gas in liquid (Davison, 2007) $m_{\text{CO}_2}(-) = \frac{C_T}{H_{\text{CO}_2\text{-water}} P}$

$$\text{Henry's constant } H_{\text{CO}_2\text{-water}} \left(\frac{\text{mol}}{\text{m}^3 \text{ bar}} \right) = 3.54 \times 10^{-7} \exp\left(\frac{2044}{T}\right)$$

- Logarithmic mean diameter $d_{lm} (m) = \frac{d_o - d_i}{\ln(d_o/d_i)}$

Table 11 shows the parameters used to calculate the theoretical overall mass transfer coefficient.

Table 11: Parameters used to calculate the theoretical overall MTC

Parameter	Unit	Value
Henry's constant (H)	$\text{mol}/\text{m}^3 \text{ bar}$	(Davison, 2007)
Solvent total concentration (C_T)	mol/m^3	1000
Fiber inner diameter (d_i)	m	2.5E-4
Fiber outer diameter (d_o)	m	6.5E-4
Temperature (T)	K	295

Sample calculations:

For the gas flowing at a flow rate of 2000 mL/min and aqueous sodium hydroxide flowing at a flow rate of 20 mL/min, the solubility of gas in liquid as function of pressure for both modules (A) and (B) was calculated as follow:

$$\text{Henry's constant: } H_{CO_2\text{-water}} \left(\frac{\text{mol}}{\text{m}^3 \text{ bar}} \right) = 3.54 \times 10^{-7} \exp \left(\frac{2044}{295} \right) * 10^5 = 36.15$$

$$\text{The solubility of gas in liquid } m_{CO_2} (-) = \frac{1000 \frac{\text{mol}}{\text{m}^3}}{(36.15 \frac{\text{mol}}{\text{m}^3 \text{ bar}}) (1 \text{ bar})} = 27.66$$

$$\text{The logarithmic mean diameter } d_{lm} (m) = \frac{(6.5E-4 - 2.5E-4)(m)}{\ln(6.5E-4/2.5E-4)} = 4.19E - 4$$

B.2 The individual mass transfer coefficient

B.2.1 Mass transfer coefficient in the tube side

Leveque's correlation (Martin, 2002) was used to describe the transfer of the fluid (gas) in the tube side. The correlation is described by Sherwood's number as follow:

$$Sh = \frac{K_G d_i}{D_{CO_2-g}} = 1.62 \left(\frac{d_i}{L} Re Sc \right)^{0.33} \quad \text{Equation 13}$$

Where Re is Reynold's number and Sc is Schmidt number and the two numbers are dimensionless (Cussler, 2009).

- Reynolds's number $Re(-) = \frac{v d_i}{\nu}$

$$\text{Fluid velocity } v \left(\frac{m}{s} \right) = \frac{GFR}{A_{in}}$$

$$\text{Fiber inner area (CS) } A_{in}(m^2) = \pi \text{ No. of fibers } \frac{(d_i)^2}{4}$$

- Schmidt number $Sc(-) = \frac{\nu}{D_{CO_2-g}}$

Table 12 shows the parameters used to calculate Leveque's correlation.

Table 12: Parameters used to calculate Leveque's correlation

Parameter	Unit	Value
Fiber inside diameter (d_i)	m	0.65E-3
Gas flow rate (GFR)	m^3 / s	3.33E-5
No. of fibers	(-)	300
Kinematic viscosity (ν)	m^2 / s	
Diffusion coefficient (D_{CO_2-g})	m^2 / s	(R.B. Bird, 1960)

Sample calculations:

For the gas flowing at a flow rate of 2000 mL/min and aqueous sodium hydroxide flowing at a flow rate of 20 mL/min, the individual mass transfer coefficient in the tube side for both modules (A) and (B) was calculated as follow:

$$\text{Fiber inner area (CS): } A_{in}(m^2) = \pi 300 \frac{(0.65E-3m)^2}{4} = 1.47E - 5$$

$$\text{Fluid velocity: } v \left(\frac{m}{s} \right) = \frac{3.33E-5 \frac{m^3}{s}}{1.47E-5 m^2} = 2.26$$

$$\text{Mass transfer coefficient in tube side: } K_G \left(\frac{m}{s} \right) = \frac{D_{CO_2-g}}{d_i} * 1.62 \left(\frac{d_i^2 v}{L D_{CO_2-g}} \right)^{0.33}$$

$$K_G \left(\frac{m}{s} \right) = \frac{1.66E - 5 \frac{m^2}{s}}{0.65E - 3 m} * 1.62 \left(\frac{(0.65E - 3 m)^2}{(0.18 m) \left(1.66E - 5 \frac{m^2}{s} \right)} \right)^{0.33} = 3.89E - 2$$

The value of mass transfer coefficient in tube side (K_G) will vary as function of pressure.

B.2.2 Mass transfer coefficient in membrane side

Individual mass transfer coefficient accounts for membrane part where it's described by (Kreulen, Smolders, Versteeg, & Van Swaaij, 1993):

$$K_M = \frac{D_{g,eff} \varepsilon}{\tau \delta} \quad \text{Equation 14}$$

Where $D_{g,eff}$ is the effective diffusion coefficient of gas (CO_2) in the gas mixture ($m^2 s^{-1}$), ε is the porosity of the membrane (-), τ is tortuosity of membrane (-) and δ is membrane thickness (m).

- Tortuosity $\tau(-) = \frac{(2-\varepsilon)^2}{\varepsilon}$ (Mackie & Meares, 1955).
- The effective diffusion coefficient of gas $D_{g,\text{eff}} \left(\frac{\text{m}^2}{\text{s}}\right) = \left(\frac{1}{D_{g,m}} + \frac{1}{D_{g,Kn}}\right)^{-1}$ (Cussler, 2009)

Where $D_{g,m}$ is the gas molecular diffusion coefficient ($\text{m}^2 \text{s}^{-1}$) and $D_{g,Kn}$ is the gas Knudsen diffusion coefficient ($\text{m}^2 \text{s}^{-1}$).

The gas molecular diffusion coefficient ($D_{g,m}$) was the same as the gas diffusion in gas mixture (D_{CO_2-g}) mentioned in Appendix (B) section B.2.1.

The Knudsen diffusion coefficient: $D_{g,Kn} \left(\frac{\text{m}^2}{\text{s}}\right) = 48.5d_p \left(\frac{T}{M_A}\right)^{0.5}$

For gas Knudsen diffusion coefficient, the Knudsen number was calculated to evaluate the importance of Knudsen diffusion coefficient (Cussler, 2009).

- Knudsen number $Kn (-) = \frac{\lambda}{d_p}$

Where λ is the mean free path $\lambda(\text{cm}) = \frac{4\kappa T}{\pi\sigma^2 P}$ and d_p is the pore diameter (μm).

Table 13 shows the constants used to calculate Knudsen number.

Table 13: Parameters used to calculate mass transfer in membrane side

Parameter	Unit	Value
Boltzmann constant (κ)	(-)	1.38E-23
Lennard-Jones parameter (σ)	(m)	3.94E-10
Pore diameter (d_p)	(μm)	0.89
Porosity (ϵ)	(-)	0.568
Thickness (δ)	(m)	2.00E-4

Sample calculations:

For the gas flowing at a flow rate of 2000 mL/min and aqueous sodium hydroxide flowing at a flow rate of 20 mL/min, the individual mass transfer coefficient in the membrane side for both modules (A) and (B) was calculated as follow:

$$\text{Tortuosity } \tau = \frac{(2-0.568)^2}{0.568} = 3.61$$

$$\text{The mean free path: } \lambda (m) = \frac{4(1.38E-23)(295K)}{\sqrt{2}\pi(3.94E-10)^2(101325)} = 5.8E - 8 \approx 0.058 \mu m$$

$$\text{Knudsen number: } k_n = \frac{0.058}{0.89} = 0.065$$

The Knudsen number calculated was 0.065 ($k_n < 1$) which in this case both diffusion should be counted and the effective diffusion coefficient is used.

$$\text{Knudsen diffusion coefficient: } D_{g,Kn} \left(\frac{m^2}{s}\right) = 48.5 * (0.89E - 6m) * \left(\frac{295}{44.01}\right)^{0.5} = 1.11E - 4$$

$$\text{The effective diffusion coefficient of gas: } D_{g,eff} \left(\frac{m^2}{s}\right) = \left(\frac{1}{1.66E-5} + \frac{1}{1.11E-4}\right)^{-1} = 1.44E - 5$$

$$\text{Mass transfer coefficient in membrane side } K_M \left(\frac{m}{s}\right) = \frac{1.44E-5}{(3.61)(2.00E-4)} = 1.14E - 2$$

The value of mass transfer coefficient in membrane side (K_M) will vary as function of pressure.

B.2.3 Mass transfer coefficient in shell side- without beads.

The last correlation used is for the individual mass transfer coefficient in the liquid phase which is defined by Yang and Cussler correlation (Cussler, 2009).

$$Sh = \frac{K_L d_h}{D_{CO_2-L}} = 1.25 \left(\frac{d_h}{L} Re \right)^{0.93} (Sc)^{0.33} \quad \text{Equation 15}$$

Where d_h is the hydraulic diameter (m) and D_{CO_2-L} is the diffusion coefficient of gas (CO_2) in the solvent ($m^2 s^{-1}$).

- Hydraulic diameter $d_h (m) = \frac{(d_{shell}^2 - No.of\ fibers * d_o)}{d_{shell} + (No.of\ fibers * d_o)}$
- Reynolds's number $Re(-) = \frac{v d_h}{\nu}$

$$\text{Fluid velocity } v \left(\frac{m}{s} \right) = \frac{LFR}{A_{in}}$$

$$\text{Fiber outer area (CS) } A_{out} (m^2) = \pi \frac{(d_{shell})^2 - No.of\ fibers (d_o)^2}{4}$$

$$\text{Kinematic viscosity } \nu \left(\frac{m^2}{s} \right) = \frac{\mu}{\rho}$$

- Schmidt number $Sc(-) = \frac{\nu}{D_{CO_2-L}}$

Table 14 shows parameters used to calculate hydraulic diameter.

Table 14: Parameters used to calculate hydraulic diameter

Parameter	Unit	Value
Shell diameter (d_{shell})	m	2.01E-2
Fiber outer diameter (d_o)	m	0.65E-3
No. of fibers	(-)	300
Diffusion coefficient (D_{CO_2-L})	m^2 / s	(Faiz & Al-Marzouqi, 2011)
Liquid flow rate (LFR)	m^3 / s	3.33E-7
Dynamic viscosity (μ)	$Kg / m^2 s$	1.37E-5
Fluid Density (ρ)	Kg / m^3	1.87

Sample calculations:

For the gas flowing at a flow rate of 2000 mL/min and aqueous sodium hydroxide flowing at a flow rate of 20 mL/min, the individual mass transfer coefficient in the shell side for module (A) was calculated as follow:

$$\text{Hydraulic diameter } d_h(m) = \frac{(2.01E-2m)^2 - (300 * (0.65E-3m))}{(2.01E-2m) + (300 * (0.65E-3m))} = 1.29E - 3$$

$$\text{Fiber outer area (CS) } A_{out}(m^2) = \pi \frac{(2.01E-2m)^2 - 300 (0.65E-3m)^2}{4} = 2.18E - 4$$

$$\text{Fluid velocity } v \left(\frac{m}{s} \right) = \frac{3.33E-7 \frac{m^3}{s}}{2.18E-4 m^2} = 1.53E - 3$$

$$\text{Kinematic viscosity } \nu \left(\frac{m^2}{s} \right) = \frac{1.37E-5 \frac{Kg}{m^2 s}}{1.87 \frac{Kg}{m^3}} = 7.34E - 6$$

$$\text{Mass transfer coefficient in shell side: } K_L \left(\frac{m}{s} \right) = \frac{D_{CO_2-L}}{d_h} * 1.25 \left(\frac{(d_h)^2 v}{L \nu} \right)^{0.93} \left(\frac{\nu}{D_{CO_2-L}} \right)^{0.33}$$

$$K_L \left(\frac{m}{s} \right) = \frac{1.38E - 9 \frac{m^2}{s}}{1.29E - 3 m} * 1.25 \left(\frac{(1.29E - 3 m)^2 \left(1.53E - 3 \frac{m}{s} \right)}{(0.18 m) \left(7.34E - 6 \frac{m^2}{s} \right)} \right)^{0.93} \left(\frac{7.34E - 6 \frac{m^2}{s}}{1.38E - 9 \frac{m^2}{s}} \right)^{0.33}$$

$$= 6.97E - 8$$

The value of mass transfer coefficient in shell side (K_G) will remain constant since the fluid is incompressible.

- In order to evaluate the Enhancement factor, Hatta number and the modified asymptotic infinite enhancement factor should be calculated first.

$$H_a = \frac{\sqrt{k_{m,n} D_A C_{A,i}^{m-1} C_{B,o}^n}}{K_L} \quad \text{Equation 16}$$

Where m and n are the partial reaction order with respect to A and B respectively, $k_{m,n}$ is the reaction rate constant ($m^3 \text{ mol}^{-1} \text{ s}^{-1}$), D_A is the diffusion coefficient of gas (CO_2) in the solvent ($m^2 \text{ s}^{-1}$), $C_{A,i}^{m-1}$ is the concentration of species A to the liquid (at the interface) (mol m^{-3}), $C_{B,o}^n$ is the concentration of species B in the liquid (mol m^{-3}) and K_L is the individual mass transfer coefficient in the liquid phase ($m \text{ s}^{-1}$).

$$E_{\infty}^* = \left(1 + \frac{C_{B,o} D_B}{v_B C_{A,i} D_A} \right) \left(\frac{D_A}{D_B} \right)^n \quad \text{Equation 17}$$

Where v_B is the stoichiometric coefficient of component B in the reaction and n depend on the type of mass transfer model used (in our case the film model is used and n=0).

The concentration of species A at the interface: $C_{A,i} \left(\frac{\text{mol}}{m^3} \right) = m_{CO_2} * C_{A,o}$

Where $C_{A,o}$ is the initial concentration of species A: $C_{A,o} \left(\frac{\text{mol}}{m^3} \right) = \frac{y_{A,o} P}{RT}$

After calculating Hatta number and asymptotic infinite enhancement factor, the division of asymptotic infinite enhancement factor over Hatta number will evaluate the limiting step (whether it's the diffusion step or reaction step) as follow:

If $\frac{E_{\infty}^*}{H_a} > 50$, then $E = \sqrt{1 + H_a^2} = H_a$ and the diffusion of Solvent is not the limiting.

If $\frac{E_{\infty}^*}{H_a} < 50$, then $E = E_{\infty}$ and the diffusion of solvent is the limiting.

If $0.02 \leq \frac{E_{\infty}^*}{H_a} \leq 50$, then $E = \frac{H_a \sqrt{(E_{\infty} - E)/(E_{\infty} - 1)}}{\tanh(H_a \sqrt{(E_{\infty} - E)/(E_{\infty} - 1)})}$ and there will be partial limitation of solvent diffusion.

Table 15 shows parameters used to calculate Hatta number and enhancement factor.

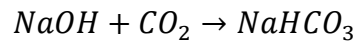
Table 15: Parameters used to calculate Hatta number and enhancement factor

Parameter	Unit	Value
Reaction rate constant ($k_{m,n}$)	$m^3/mol s$	(Zanfir, Gavriilidis, Wille, & Hessel, 2005)
Concentration of species B in the liquid ($C_{B,o}$)	mol/m^3	1000
Diffusion coefficient of CO ₂ in the solvent (D_A)	m^2 / s	1.78E-09
Diffusion coefficient of NaOH in the solvent (D_B)	m^2 / s	8.92E - 10
individual MTC in liquid phase (K_L)	m / s	6.97E - 8
Mole fraction of CO ₂ ($y_{A,o}$)	(-)	0.05
Gas constant (R)	$m^3 atm / K mol$	8.21E - 5
Temperature (T)	K	295

Sample calculations:

For the gas flowing at a flow rate of 2000 mL/min and aqueous sodium hydroxide flowing at a flow rate of 20 mL/min, Hatta number for both modules (A) and (B) was calculated as follow:

According to (Yoo, Han, & Wee, 2013), the chemical reaction of NaOH with CO₂ is:



The value of $m=1$ and $n=1$ and Hatta number will be:

$$\text{Hatta number: } H_a = \frac{\sqrt{k_{1,1} D_{CO_2-L} C_{NaOH-L,0}^1}}{K_L}$$

$$H_a = \frac{\sqrt{(6.94 \frac{m^3}{mol \cdot s}) (1.78E - 9 \frac{m^2}{s}) (1000 \frac{mol}{m^3})}}{(6.97E - 8 \frac{m}{s})} = 18978$$

The asymptotic infinite enhancement factor: $E_{\infty}^* = \left(1 + \frac{C_{B,0} D_B}{v_B C_{A,i} D_A}\right) \left(\frac{D_A}{D_B}\right)^n$

The value of $n = 1$ and $v_B = 1$.

The initial concentration of species A: $C_{A,0} \left(\frac{mol}{m^3}\right) = \frac{0.05 * 1 \text{ atm}}{\left(8.21E-5 \frac{m^3 \cdot atm}{K \cdot mol}\right) (295K)} = 2.07$

The concentration of species A at the interface: $C_{A,i} \left(\frac{mol}{m^3}\right) = 27.66 * 2.07 \left(\frac{mol}{m^3}\right) = 57.13$

$$E_{\infty}^* = \left(1 + \frac{\left(1000 \frac{mol}{m^3}\right) (8.92E - 10 \frac{m^2}{s})}{\left(57.13 \frac{mol}{m^3}\right) (1.78E - 9 \frac{m^2}{s})}\right) \left(\frac{1.78E - 9 \frac{m^2}{s}}{8.92E - 10 \frac{m^2}{s}}\right)^1 = 9.75$$

Hatta number was calculated and found to be 18978 whereas the asymptotic infinite enhancement factor was found to be 9.75. The division of the asymptotic infinite enhancement factor by Hatta number was $5.14E-04$ which means $E_{\infty}^* = E$

B.2.4 Mass transfer coefficient in shell side- with beads.

Two correlations were used to calculate the individual mass transfer coefficient in the liquid phase. The first one is the same as the one defined by Yang and Cussler correlation (Marzouk et al., 2012) which is correlation 6. The only difference here is the calculation of the velocity of the liquid in shell side packed with beads.

To calculate the velocity in shell side packed with beads:

The specific gravity of glass beads $SG = \frac{\rho_{GB}}{\rho_{H2O}}$

Where: ρ_{GB} is the glass beads density (kg m^{-3}), ρ_{H2O} is the water density (kg m^{-3}).

The volume of beads $V (m^3) = \frac{m}{\rho_{GB}}$

Where: m is the mass of glass beads (g).

The shell volume without beads $V_{shell}(m^3) = \frac{\pi L}{4} (d_{shell}^2 - No. of fibers * (d_o)^2)$

Where: d_{shell} is the shell diameter (m), d_o is the fiber outer diameter (m).

$V_{shell-with beads}(m^3) = \text{Shell volume without beads} - \text{beads's volume}$

Area of shell with beads $A (m^2) = \frac{V_{shell-with beads}}{L}$

Velocity of shell $v_{shell} \left(\frac{m}{s}\right) = \frac{LFR}{\text{area of shell with beads}}$

Table 16 shows the parameters used to calculate velocity of shell.

Table 16: Parameters used to calculate velocity of shell

Parameter	Unit	Value
Specific gravity (SG)	(-)	2.55
Water density (ρ_{H_2O})	Kg/m^3	1000
Mass of Glass beads (m)	65	65
Shell diameter (d_{shell})	m	2.00E-2
<i>No. of fibers</i>	(-)	300
Fiber outer diameter(d_o)	m	0.65E-3
Length (L)	m	0.18
Liquid flow rate (LFR)	m^3/s	3.33E-7

Sample calculations:

For the gas flowing at a flow rate of 2000 mL/min and aqueous sodium hydroxide flowing at a flow rate of 20 mL/min, velocity of shell packed with glass beads for module (B) was calculated as follow:

$$\text{The density of glass beads } \rho_{G.B} \left(\frac{g}{m^3} \right) = 10^6 \frac{g}{m^3} * 2.55 = 2550000$$

$$\text{The volume of beads } V (m^3) = \frac{65 g}{(2550000 \frac{g}{m^3})} = 2.55E - 5$$

The shell volume without beads:

$$V_{shell}(m^3) = \frac{\pi L}{4} ((2.E - 2m)^2 - (300 * (0.65E - 3m)^2)) = 3.92E - 5$$

$$V_{shell-with beads}(m^3) = 3.92E - 5m^3 - 2.55E - 5m^3 = 1.37E - 5$$

$$\text{Area of shell with beads } A \text{ (m}^2\text{)} = \frac{1.37E-5m^3}{0.18 m} = 7.60E - 5$$

$$\text{Velocity of shell } v_{shell} \left(\frac{m}{s}\right) = \frac{3.33E-7\frac{m^3}{s}}{7.60E-5m^2} = 4.38E - 3$$

The second correlation is defined by (Turchetti, 2017) :

$$Sh = 1.17 (Re)^{0.58}(Sc)^{0.33} \quad \text{Equation 18}$$

- Reynolds's number $Re(-) = \frac{\rho v_s d_{beads}}{\mu}$

$$\text{Fluid superficial velocity } v_s \left(\frac{m}{s}\right) = \frac{LFR}{A_{in}}$$

$$\text{Kinematic viscosity } \nu \left(\frac{m^2}{s}\right) = \frac{\mu}{\rho}$$

- Schmidt number $Sc(-) = \frac{\nu}{D_{CO_2-L}}$

Table 17 shows the parameters used to calculate correlation (18).

Table 17: Parameters used to calculate correlation (18)

Parameter	Unit	Value
Beads diameter (d_{beads})	m	Measured
Dynamic viscosity (ν)	$Kg/m s$	1.37E-5
Fluid density (ρ)	Kg / m^3	Reference
Liquid flow rate (LFR)	m^3 / s	3.33E-7
No. of fibers	(-)	300
Dynamic viscosity (μ)	$Kg / m^2 s$	1.37E-5
Fluid Density (ρ)	Kg / m^3	1.87

Sample calculations:

For the gas flowing at a flow rate of 2000 mL/min and aqueous sodium hydroxide flowing at a flow rate of 20 mL/min, the individual mass transfer coefficient in the shell side for module (B) was calculated as follow:

Appendix C: Calculations of CO₂ loading.

CO₂ loading is defined as the number of moles of CO₂ absorbed divided by the number of moles of absorbent (Y. E. Kim et al., 2013).

$$CO_2 \text{ loading} = \frac{n_{CO_2}}{n_{absorbent}}$$

Where: n_{CO_2} is the number of moles of CO₂ absorbed (mol) and $n_{absorbent}$ is the number of moles of solvent (mol).

The number of CO₂ moles absorbed by the absorbent is calculated from:

$$n_{CO_2(moles)} = C_{A,0} * GFR$$

Where: $C_{A,0}$ is the inlet concentration of CO₂ (mol m⁻³) and GFR is the gas flow rate (m³ s⁻¹).

The number of moles of the absorbent is calculated from:

$$n_{absorbent} = LFR * M$$

Where: LFR is the liquid flow rate (m³ s⁻¹) and M is the molarity of solvent (mol L⁻¹).

Table 18 shows the parameter needed to calculate the CO₂ loading.

Table 18: parameters to calculate CO₂ loading

Parameter	Unit	Value
$CO_{2,inlet}$	mol/m^3	2.07
Liquid flow rate (LFR)	m^3 / s	3.33E-7
Gas flow rate (GFR)	m^3 / s	3.33E-5
Molarity of solvent (M)	mol/m^3	1000

Sample calculations:

For the gas flowing at a flow rate of 2000 mL/min and aqueous sodium hydroxide flowing at a flow rate of 20 mL/min, CO₂ loading for module (B) was calculated as follow:

$$n_{CO_2}(\text{moles}) = 2.07 \frac{\text{mol}}{\text{m}^3} * 3.33E - 5 \frac{\text{m}^3}{\text{s}} = 6.89E - 5$$

$$n_{absorbent}(\text{moles}) = 3.33E - 7 \frac{\text{m}^3}{\text{s}} * 1000 \frac{\text{mol}}{\text{m}^3} = 3.33E - 4$$

$$CO_2 \text{ loading} = \frac{6.89E - 5 \frac{\text{mol}}{\text{s}}}{3.33E - 4 \frac{\text{mol}}{\text{s}}} = 0.21$$

According to the chemical reaction of NaOH with CO₂ described in appendix B (B.2.3), 1 mole of CO₂ will be absorbed by 1 mole of NaOH and CO₂ loading will be

- As the pressure and the liquid flow rate are increasing, the solvent gets saturated where the CO₂ loading will be greater than 1.